Fouling and clogging behavior of porous membrane during biogas recovery from submerged granular anaerobic membrane bioreactor permeate

Qazi Sohaib, Christophe Charmette, Jim Cartier, Geoffroy Lesage, Jean-Pierre Mericq

Fouling and Clogging Behavior of Porous Membrane During Biogas Recovery from Submerged Granular Anaerobic Membrane Bioreactor Permeate

Qazi Sohaib*, Christophe Charmette, Jim Cartier, Geoffroy Lesage, Jean-Pierre Mericq

Institut Européen des Membranes, IEM – UMR 5635, CNRS, ENSCM, Université de Montpellier, Montpellier, France

*geoffroy.lesage@umontpellier.fr, engrsohaib492@gmail.com

Abstract

This work investigated the fouling and clogging behavior of the porous polypropylene (PP) membrane during the long-term (1032 hrs.) biogas recovery operation of the ultrafiltration effluent discharged from an in-house granular anaerobic membrane bioreactor (G-AnMBR) unit. The study implemented different cleaning strategies, evaluated performance loss and recovery due to fouling and cleaning, and characterized the fouling. The normalized CH_4 flux dropped by 54 % while the liquid pressure drop increased from 10 to 800 mbar after 312 hrs. operation before cleaning. Acid cleaning (AC) was found to be very effective in removing both reversible and irreversible fouling and restoring the initial membrane performance while water cleaning (WC) and basic cleaning (BC) were inefficient. Carbonate ions, Ca^{2+}, and CO_3^{2-}, were found to be the major inorganic fouling elements. The organic fouling consisted of 79 % aromatic proteins, 17 % fulvic-like substances, and 4 % soluble microbial products. Evidence of biofouling was confirmed by COD and DOC analysis and by detecting nucleic acids in the FTIR analysis.

Keywords: Biogas recovery, Anaerobic Membrane Bioreactor, Permeate, Fouling, Clogging

1 Introduction

Wastewater is becoming an important source of fresh water and a valuable resource for renewable energy and nutrients in the form of biogas and fertilizers [1,2]. To make wastewater uses more practical, it is required to develop efficient, economical, and environmentally friendly technologies.

Anaerobic Membrane Bioreactor (AnMBR) technology, which couples the anaerobic bioreactor and membrane separation, has emerged as a promising technology for the treatment of low strength wastewater even at low temperatures (<25°C) [3–5]. Using granular biomass in a granular AnMBR (G-AnMBR) makes this process more advantageous as it has high settling capacity, high strength to loading rates, balanced bacteria consortia, and a compact biomass structure [6]. This technology is very attractive as it has low energy input requirement, an easy scale up, a reduce footprint, and a selective separation between resources and nutrients [7,8]. The AnMBR operation, during the biological reactions of organic matter degradation produces biogas. Typically, 55-60 % of the produced CH_4 joins the headspace biogas stream (composed of around 50-70 % CH_4 and CO_2 (30 – 50%), while the rest remains dissolved in the permeate, which is being discharged [9]. Similarly, a part of the produced CO_2 also remains dissolved in the discharged permeate stream.

The dissolved biogas loss is critical as it represents significant economic loss, safety concerns in the downstream processes, and environmental concerns due to the high global warming potential of both CH_4 and CO_2 [10,11]. The methane loss in the discharged permeate can increase up to 80 % of the total produced methane at lower temperatures (<15°C), which in turn can make the process very inefficient and can also increase the carbon footprint [12,13]. Normally, the dissolved methane content of the anaerobic effluent is between 10-25 mg L^{-1}, depending upon the methane partial pressure in the headspace and liquid temperature, but the supersaturation indices can be as high as 6.9 [14]. Several authors, including [15], have observed that if the dissolved methane is recovered efficiently, the whole AnMBR operation could be operated without any additional energy input. Hence, the dissolved biogas recovery is imperative for operating a more energy-efficient and environmentally friendly AnMBR system.

To recover the dissolved biogas from the AnMBR effluents, several conventional methods including spray aeration, diffused aeration, packed column, and jet tower have been tried before [16]. However, these methods develop very serious operational drawbacks including flooding, channeling, and foaming [17]. A membrane contactor can give us a promising alternative to overcome the above-mentioned drawbacks during the recovery of the dissolved biogas. This technology has been widely used for liquid degassing at lab scale as well as industrial scales [15]. Membrane contactors are compact units that provide high volumetric mass transfer coefficients by offering a transfer of gas

molecules across a porous or dense membrane without the dispersion of the two phases [18,19]. Porous membranes for the degassing process are extensively recommended as they provide low resistance to the mass transfer and therefore offer high recovery efficiencies [15,20]. However, the liquid solvent may penetrate inside the pores (wetting), which creates an unfavorable environment for the gas mass transfer. Under wetting conditions, the membrane mass transfer flux dramatically decreases and hence the degassing efficiency too [21]. The unfavorable wetting effects can be reduced by controlling the membrane module pressure drop, keeping low transmembrane pressure, increasing the hydrophobicity of the membrane, and decreasing membrane pore size [22,23]. On one hand, an increase in the hydrophobicity decreases the possibility of pore wetting, but on the other hand, it can speed up the process of membrane fouling and can affect the membrane surface morphology in long term operations, thus again increasing the possibility of pore wetting [24–26].

Performance loss due to membrane fouling is a major challenge while coupling AnMBR units and membrane degassing units. Two main fouling mechanisms could generally be expected in membrane processes and membrane contactors, namely external fouling and internal fouling [2]. External fouling, which occurs in the form of the cake layer ("reversible fouling") and/or gel layer (irreversible fouling), is caused by the deposition of particles, inorganic solutes, colloids, and macromolecules having larger sizes than of membrane pore [27]. Surface or internal fouling ("irreversible fouling") occurs due to the submersion or retention of particles, undissolved matter, and solutes inside the membrane pores but also to adsorption of compounds on membrane material. Fortunately, in membrane contactors, there is no convective flow throw through the membrane pores and there is no operating pressure applied for membrane filtration, which reduces the chances of pore plugging or clogging [28]. The Anaerobic effluents usually have 100-300 mg L^{-1} concentration of suspended solids, with 60-85% of the solids having sizes higher than 300 µm [29]. This is so likely to have a rapid membrane clogging, especially when liquid is flowing on the lumen side. The clogging issue could be a major challenge, and might be controlled by prefiltration [29]. An AnMBR unit provides the advantage of prefiltration (ultrafiltration or microfiltration) using a submerged membrane. While dealing with the AnMBR effluents, the nature of the fouling could be inorganic, organic, or biofouling. Inorganic fouling can be found in the form of scalants, inorganic colloids, or crystals that deposit or precipitate over the membrane or pore surface [30]. Organic fouling is caused due to the deposition of macromolecules such as biopolymers and organic compounds over the surface of the membrane [31]. Biofouling is caused by the interaction of membrane surface with the components of biological treatment broth and also due to the deposition of soluble microbial products (SMP) and extracellular polymeric substances (EPS) over the surface of the membrane [32].

Few literature reports have evaluated the long-term performance and fouling issue during biogas degassing from anaerobic effluents in membrane contactors. Bandara and co-workers [33] studied the membrane contactor process on long duration (but operation time was not provided clearly), by employing a composite hollow fiber membrane, consisting of a non-porous layer of polyethylene and a porous layer of polyurethane, treating the effluent of a bench-scale upflow anaerobic sludge blanket (UASB). Although, no direct experimental data was presented nor any cleaning protocols, however, it was claimed to have no indication of the significant fouling. Henares and co-workers [28] studied the long-term operation of polypropylene (PP) membrane contactor for CH_4 degassing from 40 µm prefiltered effluent of expanded granular sludge-bed (EGSB) anaerobic reactor. They revealed the fouling to be less intense and more reversible in nature while operating on the lumen side. All three types of the fouling namely organic, inorganic, and biofouling were observed. A 30 minutes daily water cleaning was recommended to prevent irreversible fouling and chemical cleaning. Rongwong and co-workers [34] studied fouling in membrane contactors for degassing CH_4 from the effluents of AnMBR and UASB, during the short time of 40 hrs. Membrane fouling was more drastic with the UASB effluent causing a greater decline in the CH_4 flux. Foulants characterization revealed cake layer formation and protein-like substances to be the major cause of fouling. No cleaning studies were reported by the author. Sethunga and co-workers [10] used a composite membrane of polyvinylidene difluoride (PVDF) coated with polydimethylsiloxane (PDMS), for CH_4 degassing from the effluents of AnMBR and UASB, for short time experiments of 10 days. Only a 20 % decline in the CH_4 flux was observed in 10 days. The study did not report the nature of the fouling nor any recommended cleaning protocols. So far, the few reports that presented the fouling in membrane contactors while degassing CH_4 from anaerobic effluents are mostly relatively short-time studies and do not present a detailed analysis of the fouling, foulants characterization, and cleaning protocols for irreversible fouling in long-term operations. Therefore, it is needed to conduct a study on the long-term membrane contactor performance for biogas degassing from the AnMBR effluent. It is also needed to study the fouling behavior and to characterize the foulants to know their nature, location, and intensity.

Previously [35], we studied the membrane contactor biogas recovery performance using both synthetic and real G-AnMBR effluent, in short term experiments (No fouling effects). Here in this work, a study was conducted to analyze the long-term membrane contactor degassing operation of the ultrafiltration effluent discharged from the submerged granular anaerobic membrane bioreactor (G-AnMBR) unit. The in-house G-AnMBR unit was in line with the membrane degassing unit. The membrane contactor was porous and made of polypropylene. The ultrafiltration effluent of the G-AnMBR unit was fed to the membrane degassing unit for the recovery of dissolved biogas. To perform the long-term analysis, the degassing operation was conducted for 1032 hrs., in total. During this

operational time, water and chemical cleaning strategies were implemented to deal with the reversible and irreversible fouling. The variations (due to fouling) in the performance parameters, including biogas flux, liquid side pressure drop, degassing and recovery efficiencies, mass transfer coefficients, and mass transfer resistances have been investigated in the long term. Various characterization techniques were implemented to identify and quantify the types of fouling and to understand the nature (organic and inorganic), intensity, and location of the foulants. It was assumed to have no development of biofouling due to the smaller G-AnMBR membrane pore size than the bacteria, thus not allowing the bacterial flow in the discharged effluent.

2 Experimental

2.1 G-AnMBR Unit and effluent

The real G-AnMBR permeate (Ultrafiltration effluent) was directly transferred to the effluent tank, from the exit of the membrane (in-house G-AnMBR bench-scale unit), using a peristaltic pump. The main characteristics of the G-AnMBR unit and discharged effluent are presented in Table 1 [6]. The G-AnMBR unit is briefly described below.

Table 1 Characteristics of the G-AnMBR unit and discharged permeate

Parameter	Value
G-AnMBR Unit	
SRT (d)	Infinite
HRT (h)	12
Organic loading rate, OLR (kg COD/m^3/d)	0.50 ± 0.14
Chemical oxygen demand, COD (mg L^{-1})	400
Total solids, TS (mg L^{-1})	50000
Volatile solids, VS (mg L^{-1})	15000
Volatile fatty acids, VFA (mg L^{-1})	130 ± 33
Membrane pore size (µm)	0.04
Temperature, T (°C)	25±2
Headspace CH_4/CO_2 ratio (-)	79.9/20.1 ± 3.5
Discharged G-AnMBR effluent	
pH (-)	7±0.3
Dissolved organic carbon, DOC (mg L^{-1})	3.25±0.5
Chemical oxygen demand, COD (mg L^{-1})	25±3
Total solids, TS (mg L^{-1})	1.70±0.2
Volatile solids, VS (mg L^{-1})	1.30±0.2
Dissolved methane, dCH_4 (mg L^{-1})	11±2

dCH_4 Oversaturation (-)	≈1
Dissolved carbon dioxide, dCO_2 (mg L^{-1})	50±10

The G-AnMBR unit was operated at ambient temperature (25°C) for the treatment of 12 L per day of complex synthetic domestic wastewater (COD/N/P = 400/11/2) [36]. The lab-scale pilot consisted of a 6 L up-flow anaerobic membrane bioreactor which integrates a submerged (in the granular sludge bed) flat sheet membrane (0.34 m²) with a 0.04 µm pore size. A hydraulic retention time of 12h and an organic loading rate of 0.5 kg COD/m^3/d were applied at steady-state before using the permeate for degassing operation. Total solids and volatile solids were measured in the mixed liquor of the G-AnMBR tank which were about 50000 mg/L and 15000 mg/L, respectively. The G-AnMBr headspace CH_4/CO_2 ratio was recorded to be 79.9/20.1.

The TS and VS contents of the discharged effluent were as low as 1.7 mg L^{-1} and 1.3 mg L^{-1}, respectively. The particulate size of the permeate was lower than 0.04 µm due to ultrafiltration with a submerged membrane. The dissolved CH_4 in the G-AnMBR permeate was found in the range of 9-13 mg L^{-1}.

2.2 Dissolved Biogas Degassing

A membrane contactor (MC) based pilot setup was developed to study the porous membrane's long-term performance and fouling behavior during biogas recovery from the G-AnMBR discharged permeate, as presented in Figure 1 below.

A porous hydrophobic membrane (3M™ Liqui-Cel™ MM-1.7x5.5) was used for degassing operations. Specifications are presented in Table 2 (provided by the manufacturer, 3M™USA). The module contained hydrophobic polypropylene hollow fibers of parallel configuration and 40% porosity, potted with polyurethane. The effective inner membrane area of the module was 0.58 m^2.

Table 2 Membrane module specifications and operating conditions

Parameter	**Value**
Membrane Contactor	
Membrane material	Polypropylene
Fiber inner diameter, d_i (m)	$2.20\ 10^{-4}$
Fiber outer diameter, d_o (m)	$3.00\ 10^{-4}$
Membrane thickness, δ (m)	$0.40\ 10^{-4}$
Effective length of the fiber, L (m)	0.11
Number of fibers, N	7400
Membrane pore diameter, d_p (m)	$4.00\ 10^{-8}$
Effective inner membrane area, A_i (m^2)	0.58

Effective outer membrane area, A_o (m^2)	0.79
Lumen side volume, V_l (mL)	53.00
Shell side volume, V_g (mL)	78.00
Porosity, ε	40.00
Packing factor, ϕ	0.36
Tortuosity, τ[a]	6.40

[a] $\tau = \frac{(2-\varepsilon)^2}{\varepsilon}$ [37]

The discharged G-AnMBR permeate was recirculated from the permeate reservoir, to the lumen side of the module, using an industrial peristaltic pump LONGER, G600-1J-1. The liquid flow rate was fixed at 100mL min^{-1} (5.93 10^{-3} m s^{-1}). The lumen side pressure drop alongside the membrane was monitored by a differential pressure transmitter, MICROSENSOR, MDM490. A sweep gas (N_2) was allowed to flow in countercurrent mode through the shell side of the module. The flow rate of the sweep gas was kept at 100 mL min^{-1} (1.86 10^{-3} m s^{-1}), using the gas flow meter, AALBORG GFC17 mass flow controller. The inlet and outlet gas side pressure were monitored by the pressure transmitter, STS ATM.ECO. The relative humidity (RH) and temperature of the gas at the module outlet were monitored by a hygro transmitter, Delta OHM HD48T. A temperature controlling jacket was used to keep the temperature of the permeate tank constant at 25°C (similar to the one at which the G-AnMBR plant was operated). For a certain operational time, the effluent was continuously recirculated in a closed loop to the reservoir. After recirculating the effluent for a certain time, it was discharged from the reservoir. A new batch of discharged G-AnMBR permeate was then transferred to the reservoir for another degassing operation. As we are studying here long-term performance and membrane fouling, the membrane degassing operation was carried out for approximately 1036 hours (43 days). During this operational time, various water and chemical cleaning strategies were also implemented (presented in the next section 2.3). The progress of the CH_4 and CO_2 desorption was monitored on both gas and liquid sides explained in the following section 2.4.

To observe the development of the fouling in the pristine membrane, especially the inorganic scalants and precipitates, a 250 mL effluent was recirculated through the pristine membrane for 72 hrs. at 400 mL min^{-1}. The initial effluent (effluent to be recirculated on the lumen side of the membrane) and 72h effluent (effluent after 72 hrs. of recirculation on the lumen side of the membrane) were then analyzed by ion-chromatography and alkalinity. The effluent in this analysis was not directly transferred for the degassing and thus was not CO_2 saturated.

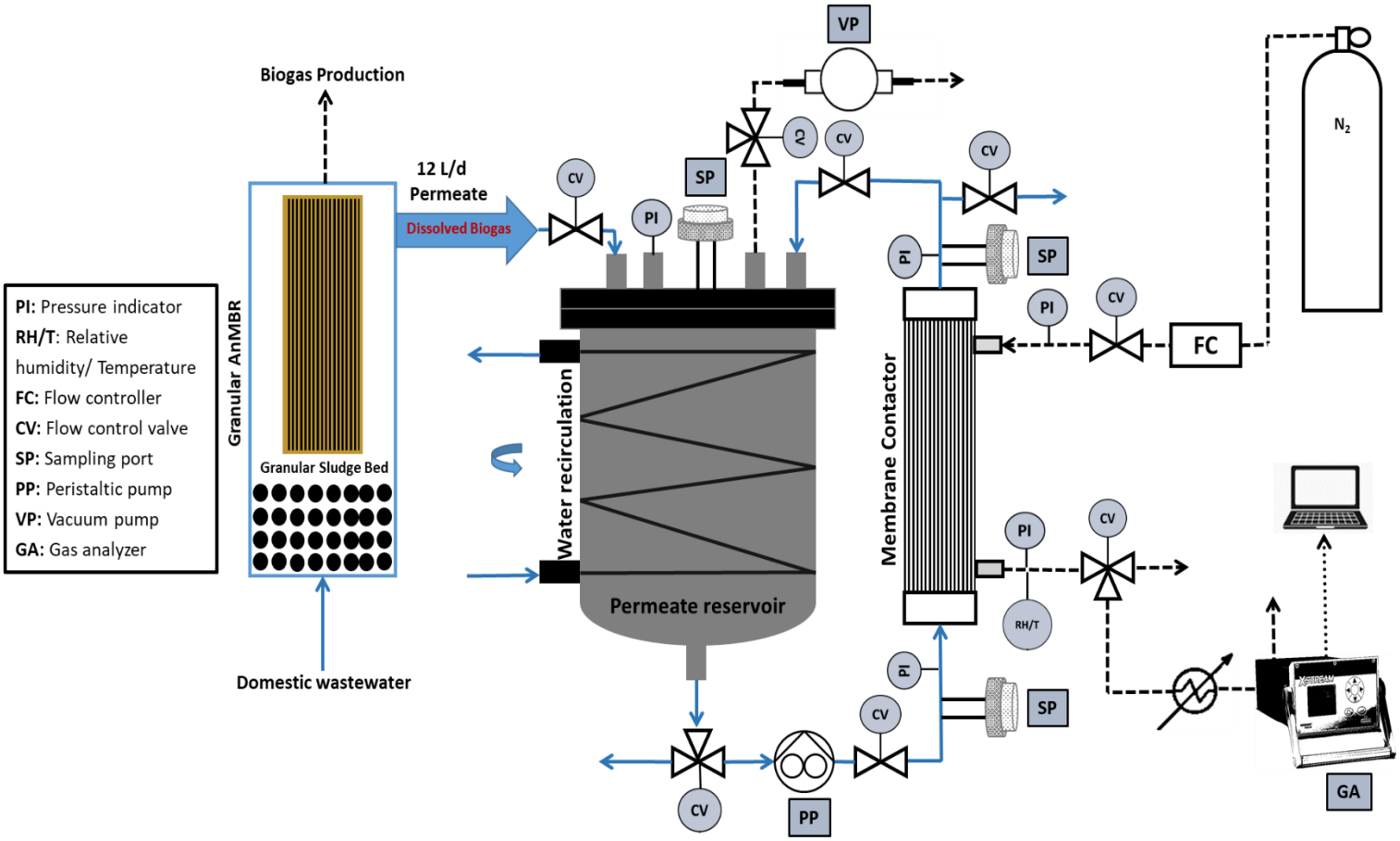

Figure 1 Membrane degassing set up in line with the granular anaerobic membrane bioreactor (G-AnMBR) unit (Solid Lines: Liquid stream; dashed lines: Gas stream)

2.3 Determination of the desorbed and dissolved biogas

Biogas concentration at the module gas outlet was measured using a biogas analyzer, Emerson X-Stream Enhanced XEGK. Before entering the gas analyzer, the gas stream was allowed to pass through a condenser, to avoid water vapors. Thus, the analyzer indicated the biogas concentration of the dry gas. Biogas concentration including water vapors (actual concentration of the biogas at the immediate gas side exit) was calculated taking into consideration the water molar fraction while using RH at the exit of the module.

$$y_{H_2O} = \frac{\%RH * p^*_{H_2O}}{100 * P} \quad (1)$$

The molar fraction of the water vapors ranged between 0.026 and 0.03. The results presented in this work are based on the wet biogas concentrations.

Biogas concentration in the liquid feed (in the permeate tank, module liquid side inlet, and outlet) was measured by the headspace method as described by various authors [28,33,38]. Gas-tight vials of 11.6

mL total volume were used (with a magnetic stirrer inside). Each vial was prepared by passing helium gas through it for 10 minutes, to evacuate the air and finally retain (inside the vial) the helium at around 100 mbar. The helium gas was selected for the preparation of vials because it was the carrier gas in the gas chromatograph used for the analysis. Gastight syringe from Hamilton, gastight 1010 were used to collect samples of 6 mL from the sampling port, and then injected through the prepared vials. The vials were then kept for stirring (~ 10 minutes) at 500 rpm and 25 °C, to acquire equilibrium. A 200 µL of the headspace gas was then collected using a 250 µL SGE gastight syringe and injected through PerkinElmer Gas Chromatograph (GC), Clarus® 680, coupled with PerkinElmer Mass Spectrometer (MS), Clarus® SQ 8 T. This mass spectrometer follows electron impact (EI) ionization for the detection. The MS Clarus® SQ 8 T identifies and quantifies compounds separated by GC Clarus® 680. A GC column RESTEK, ShinCarbon ST 100/120 of 2m length and 1 mm inner diameter was used. The Column temperature varied in the range of 40-200 °C, with an initial pressure of ~3.45 bar. The Injection port temperature was kept at 150 °C. The carrier gas (He 5.0) flowrate was 50 mL min^{-1} with a split of 40 mL min^{-1}. The gas chromatograph gives us the biogas concentration in the headspace C_{gh} (mg L^{-1}). The dissolved biogas concentration in the liquid phase C_l (mg L^{-1}), was then calculated from Equation 2.

$$C_l = \frac{C_{gh}\left(V_{gh} + {}^{V_l}/_{H}\right)}{V_l} \quad (2)$$

Where V_{gh} and V_l represent the headspace volume and the liquid volume in the vial, respectively. The term H (C^*_{gh}/ C^*_l) denotes the dimensionless Henry's law constant. This constant is used for the equilibrium between biogas concentration in the gas (C^*_{gh}) and liquid (C^*_l) phases inside the vial. The dimensionless Henry's law constant for the CH_4 and CO_2 were estimated to be 28.8 and 1.22 [39].

2.4 Performance parameters calculation

Biogas mass flux (mg m^{-2} min^{-1}) across the membrane was calculated using the molar mass of biogas M_g (mg mol^{-1}), external area of the membrane A_o (m^2), the gas concentration at the module gas side inlet $C_{g\text{-}in}$ (mg L^{-1}), the gas concentration at the module gas side outlet $C_{g\text{-}out}$ (mg L^{-1}), gas flowrate at the module gas side inlet $Q_{g\text{-}in}$ (mL min^{-1}), and gas flowrate at the module gas side outlet and $Q_{g\text{-}out}$ (mL min^{-1}). The equation is presented below (Equation 3).

$$N = \frac{Q_{g-out}C_{g-out} - Q_{g-in}C_{g-in}}{Mg\ A_o} \quad (3)$$

The membrane degassing efficiency was calculated using dissolved biogas concentration at the module liquid side inlet $C_{l\text{-}in}$ (mg L^{-1}) and outlet $C_{l\text{-}out}$ (mg L^{-1}) as of Equation 4.

$$Degassing\ efficiency = \frac{C_{l-in} - C_{l-out}}{C_{l-in}} * 100 \quad (4)$$

Biogas recovery (%) over some time t, was calculated from the dissolved biogas concentration (initial= C_{l-i}, after time t=C_{l-t}) in the effluent tank following Equation 5.

$$\%\ Recovery_t = \frac{C_{l-i} - C_{l-t}}{C_{l-i}} * 100 \quad (5)$$

The overall experimental mass transfer coefficient, K_{exp} (m s^{-1}), was calculated from the following equation;

$$K_{exp} = \frac{Q_l (C_{l-in} - C_{l-out})}{A_i \Delta C_{lm}} \quad (6)$$

Where A_i (m^2) is the internal area of the membrane and ΔC_{lm} is the logarithmic mean of the driving force, which can be calculated from Equation 7;

$$\Delta C_{lm} = \frac{(C_{l-in} - C^*_{l-in}) - (C_{l-out} - C^*_{l-out})}{\ln\left(\frac{C_{l-in} - C^*_{l-in}}{C_{l-out} - C^*_{l-out}}\right)} \quad (7)$$

Where $C^*_{l\text{-}in}$ ($C^*_{l\text{-}in}$= $C_{g\text{-}out}$/H) is the liquid phase inlet biogas concentrations in equilibrium with the gas phase outlet concentration ($C_{g\text{-}out}$) and $C^*_{l\text{-}out}$ ($C^*_{l\text{-}out}$= $C_{g\text{-}in}$/H) is the liquid phase outlet biogas concentrations in equilibrium with the gas phase inlet ($C_{g\text{-}in}$=0) concentration.

The resistance generated due to fouling, R_f (s.m^{-1}) was calculated from the experimental mass transfer coefficient of the pristine membrane at time 0, $K_{exp,0}$, and after developing the fouling at a certain time t, $K_{exp,t}$. The equation is presented below.

$$R_f = \frac{1}{K_{exp,t}} - \frac{1}{K_{exp,0}} \quad (8)$$

2.5 Membrane cleaning strategies

Different cleaning strategies were implemented during the long-term degassing operation of this work, presented in Table 3 below. These strategies include membrane header cleaning (HC), water cleaning (WC), acid cleaning (AC), and basic cleaning (BC). Deionized water was used for HC, WC, and also for making solutions for AC and BC. Details of each cleaning mode are presented in Table 3. In the HC, the membrane header was opened (the header was removable) and cleaned with deionized water. The header foulants (H-Foulants) were collected for further analysis. Acid and basic cleanings were respectively performed by using citric acid and sodium hydroxide solutions. Water cleanings were always performed in the single-pass mode (water passed only once through the membrane) while chemical cleanings were performed in recirculation modes. In the case of AC and BC, after each cleaning recirculation, the membrane was washed by a single pass of 2 L of deionized water at 400 mL.min^{-1}. Other than the methods mentioned in Table 3, a reverse liquid flow (RLF) method was also

implemented. During the RLF the membrane module inlet and outlets were inverted during the degassing operation to remove the reversible fouling and clogging on the membrane header sides.

Table 3 Membrane cleaning modes

Property	Header cleaning (HC)	First (WC1) and second (WC2) water cleaning	First acid cleaning (AC1)	Second acid cleaning (AC2)	First basic cleaning (BC1)	Second basic cleaning (BC2)
Solvent type	Deionized water	Deionized water	Citric acid solution	Citric acid solution	Sodium hydroxide solution	Sodium hydroxide solution
Solvent Volume	500 mL	5000 mL	1500 mL	1000 mL	1500 mL	1500 mL
Concentration	-	-	10 % w/w	10 % w/w	2 % w/w	3 % w/w
Flowrate	-	400 mL min^{-1}	400 mL min^{-1}	400 mL min^{-1}	100 mL min^{-1}	100 mL min^{-1}
Flow mode	-	Single-pass, reverse flow	Recirculation, 1hr	Recirculation, 1hr	Recirculation, 1hr	Recirculation, 1hr

2.6 Membrane fouling and foulants characterization

Effluent, membrane fouling and foulants were characterized using different characterization techniques. These techniques were implemented as described below.

The membrane morphological changes and fouling due to long-term contact with the G-AnMBR permeate were studied using fiber immersed in discharge G-AnMBR effluent for one or five months. Fibers were then analyzed with a scanning electron microscope, Hitachi S-4800 FE-SEM. Prior to SEM analysis, samples were sputter-coated with platinum for 5 minutes to ensure better conductivity. Samples were observed at an acceleration voltage of 2kv.

Energy Dispersive X-Ray Analysis (EDX), was performed to identify the elements inside the pristine membrane fiber, fouled membrane fiber, and membrane header foulants (H-Foulants). H-Foulants are the foulants that were developed in the header of the membrane and were cleaned using deionized water. It was oven-dried after (at 50°C) and was kept in the form of powder. For the EDX analysis, the weight / atomic percentages in the samples were determined by EDX using a Zeiss SEM EVOHD15 at 10 kV with the Oxford instruments software. Samples were deposited on double-sided carbon tape and coated with Pt.

Inorganic foulants in the initial effluent and 72h effluent (recirculation of 250 mL effluent on the lumen side of the membrane at 400 mL min^{-1}), H-Foulants, and post-acid cleaning solution (cleaning solution recovered after the acid cleaning procedure) were quantified by the technique of ionic chromatography. To dissolve inorganic salts and scalants from the header fouling, 50 mg of H-Foulants were added to 3 mL of deionized water and were shaken for 1 hr. Before the analysis, samples were

filtrated at 0.22 µm. The anion analysis was performed using Dionex ICS-1000, USA, equipped with an IonPac AS19 column. The cation analysis was performed Using Dionex ICS-900, USA, equipped with an IonPac CS12A column. The quantification was performed by conductivity.

COD of the G-AnMBR effluent and H-Foulants were measured using HACH pre-dosed photochemical Cuvette LCK 1414, Germany. For the H-Foulants organic matter extraction, 100 mg of the H-Foulants were added to 20 mL of 0.11 M KCL solution. The solution was well shacked for 2hrs. at 200 rpm using DLAB SK-L330-Pro, and was filtrated at 0.22 µm, after extraction. Samples were then, transferred to the vials and heated at 150 °C for 2 hrs, in a thermoreactor, Spectroquant® TR 420, for digestion. After digestion, the samples were cooled down to room temperature and COD was measured using Hach UV-Vis spectrophotometer DR3900, Germany.

DOC of the G-AnMBR effluent and H-Foulants were analyzed for samples pre-filtered at 0.22 µm by a TOC analyzer, TOC-V_{CSN}, Shimadzu Corporation, Japan. The organic matter of the H-Foulants was extracted by the method described above.

Florescence spectra (3DEEM) of the G-AnMBR effluent, H-Foulants, and post-AC solution were obtained using Perkin-Elmer LS-55 spectrometer, USA. The H-Foulants organic matter was extracted as mentioned in the COD measurement section above. The samples were pre-filtered at 0.22 µm and were analyzed in pure and also in diluted format. Dilutions were performed by adding ultra-pure water Milli-Q, Millipore Co. Ltd., to limit overlapping signals [40]. G-AnMBR effluent was diluted 20 times, H-Foulants organic matter extracted KCL solution was diluted 10 times, and post-AC solution was diluted 5 times. The excitation and emission scan ranges were respectively fixed at 200-500 nm and 280-600 nm, to cover a wide range of organic species [41]. The scan speed was fixed at 1000 nm min^{-1} and the slit width was fixed at 10 nm. Blanks were also analyzed in the same conditions using Milli-Q water. Further details about the integration and quantification are available from [42]. The 3DEEM and the volume of fluorescence (in arbitrary unit per nm^2 (A.U/nm^2)) beneath each region were obtained according to [42]. The volume gave us semi-quantitative information about the number of fluorophores present in each region.

The FTIR analysis of the oven-dried H-Foulants was performed using ThermoFisher Nexus and Nicolet 710 FTIR Spectrometer, having separator Ge/KBr (7400-350 cm^{-1}) and detector MCTA (11700-600 cm^{-1}). The FTIR spectrometer was used along with the accessory DuraSamplIR II.

3 Results and Discussion

3.1 Porous membrane performance loss and recovery; long-term analysis

A membrane contactor degassing operation was performed for 1032 hours. Due to continuous operation (without continuous cleaning procedure) of the G-AnMBR effluent degassing, the membrane contactor developed fouling and performance loss. During this long-term investigation, the performance was partially or totally restored by removing the reversible or irreversible fouling, using water cleaning or chemical cleaning, respectively. The performance loss and recovery of the porous membrane contactor were evaluated using various performance parameters including biogas flux, liquid side pressure drop, degassing and recovery efficiencies, mass transfer coefficients, and mass transfer resistances.

3.1.1 Transmembrane flux and liquid side pressure drop

Biogas flux was calculated as of equation 3 and has been presented in Figure 2 below. The figure presents the loss and recovery of the biogas flux due to membrane fouling and cleaning, respectively. CH_4 flux is presented here and CO_2 flux is available from Figure S1 of the supplementary data. The flux values are normalized with the initial flux of the pristine membrane (flux at time t N_t divided by initial fluxN_0) to easily enlighten flux variations. Figure 2 also describes the long-term variations in the liquid side pressure drop (liquid on the lumen side of the membrane), i.e., a pressure difference generated between the liquid inlet and outlet due to flow resistance (and potential flow clogging).

Figure 2 was divided into three periods for better understanding. Period 1 (white background) presented the pristine membrane fouling for a continuous 312 hrs. operation without cleaning. For the pristine membrane, the initial liquid side pressure drop was about 10 mbar and the increase in the pressure drop (due to fouling and clogging) was initially, very slow. A significant drop in the normalized biogas flux, as well as a huge increase in the liquid side pressure drop, was next observed after around 168h and until 312 hrs. of the operation, before implementing the first water cleaning step. The drop in the normalized flux was recorded to be 54 % for CH_4 and 50 % for CO_2, while the liquid side pressure drop increased from initially 10 mbar to 800 mbar. The increase in the pressure drop during period 1 represented an average fouling rate of 61 mbar day^{-1}. During this first period, two reverse liquid flow (RLF) at time 48 hrs. (RLF1) and time 264 hrs. (RLF2) were implemented. RFLF were adopted mainly to avoid and/or reduce reversible clogging. We can observe that the first reverse liquid flow (RLF1) had no significant effect on both biogas flux and liquid side pressure drop (no significant clogging at this time), while the second one (RLF2) induce only a temporary slight recovery of 92 mbar of pressure drop in the liquid side.

RLF was not efficient enough and after pristine membrane fouling in Period 1, two water cleaning (WC) and one acid cleaning (AC) were performed during Period 2 (gray color). Firstly, a header cleaning (HC) and water cleaning (WC1) were performed, for which the protocols are explained in Section 2.5. This cleaning step increased the CH_4 and CO_2 normalized flux by 67 % and 24 %, while the liquid side pressure drop decreased from 800 mbar to 130 mbar. The improvement in the performance could be possibly due to the removal of reversible fouling (more than for the RLF). As both flux and pressure drop were not restored to their initial values, there could be a possible development of irreversible fouling and/or clogging inside the module. Henares and co-workers [28] have also reported similar results of the not fully effective water cleaning. After WC1, the flux again started dropping while the liquid side pressure drop was increasing, until WC2 was performed. With WC2, the CH_4 and CO_2 normalized flux increased by 26 %, and 32 %, respectively, while the liquid side pressure drop decreased from 900 mbar to 120 mbar. The average fouling rate in this period was recorded to be 128 mbar day^{-1}. A first acid cleaning (AC1) was performed after 552 hrs. of the operation to deal with the irreversible fouling and the CH_4 flux was increased by 85 %. After AC1, the CH_4 flux was recovered as of the initial value of the pristine membrane while the CO_2 normalized flux was recorded to be slightly higher (1.2) than the initial one. This could be either due to the supersaturation level of the effluent or due to the acid treatment of the membrane which might have affected the pH over the membrane surface and also the CO_2 release from the effluent. The liquid side pressure drop also decreased to nearly its initial value. The AC was very efficient and could possibly remove both reversible and irreversible fouling. This also confirmed the existence of a huge amount of inorganic foulants. It can also be attributed that AC might have been able to remove the inorganic fouling as well as organic fouling (possibly major components of the organic foulants). The removal of organic foulants by AC was also confirmed by others [43]. The study described that AC (with citric acid) can remove mineral scales and metal oxides, but can also solubilize organic foulants through micelle formation. It was also mentioned that AC can remove fats, oils, and biological foulants too. The recovery of the liquid side pressure drop with AC indicated that the fiber clogging could be dominantly caused due to the inorganic scalants and precipitates.

Period 3 (yellow color) begins after the acid cleaning. Toward the end of this period, two basic cleanings (BCs) and finally one more AC were performed. After the first AC at the end of Period 2, the membrane was continuously operated without cleaning, until 912 hrs. of the operation when the first basic cleaning (BC1) was performed. The average fouling rate during this time was recorded to be 69 mbar day^{-1}. The BC1 increased the CH_4 and CO_2 normalized flux by 30 % and 9 %, while the liquid side pressure drop decreased from nearly 1000 mbar to 150 mbar. However, the BC was not able to recover the initial flux and pressure drop. This could be attributed that BC1 only removed totally the reversible

fouling but not all of the irreversible fouling. The study of Brant and co-workers [43] described that BC (with NaOH) was able to solubilize organics, polysaccharides, proteins, and biological foulants but was ineffective in removing Ca^{2+}/organic complexes. This explains and justifies the ineffectiveness of the BC to completely recover the biogas flux in our work. To verify this, another basic cleaning (BC2) was performed with a high concentration of sodium hydroxide, at 960 hrs. of the operation. No further flux recovery was observed. Here at this stage, the membrane header experienced cracks due to a very high liquid side pressure drop of 1200 mbar. Finally, at 1008 hrs. of the operation another acid cleaning, (AC2) was performed, which again recovered both flux and liquid side pressure drop to its initial values. Henares [28] have also reported the recovery of the membrane performance with chemical cleaning. However, the study was short (nearly 600 hrs.) as compared to our study and the author reported performance recovery after combining AC and BC. Due to the combination of AC and BC it was not possible to conclude which cleaning was more effective against fouling.

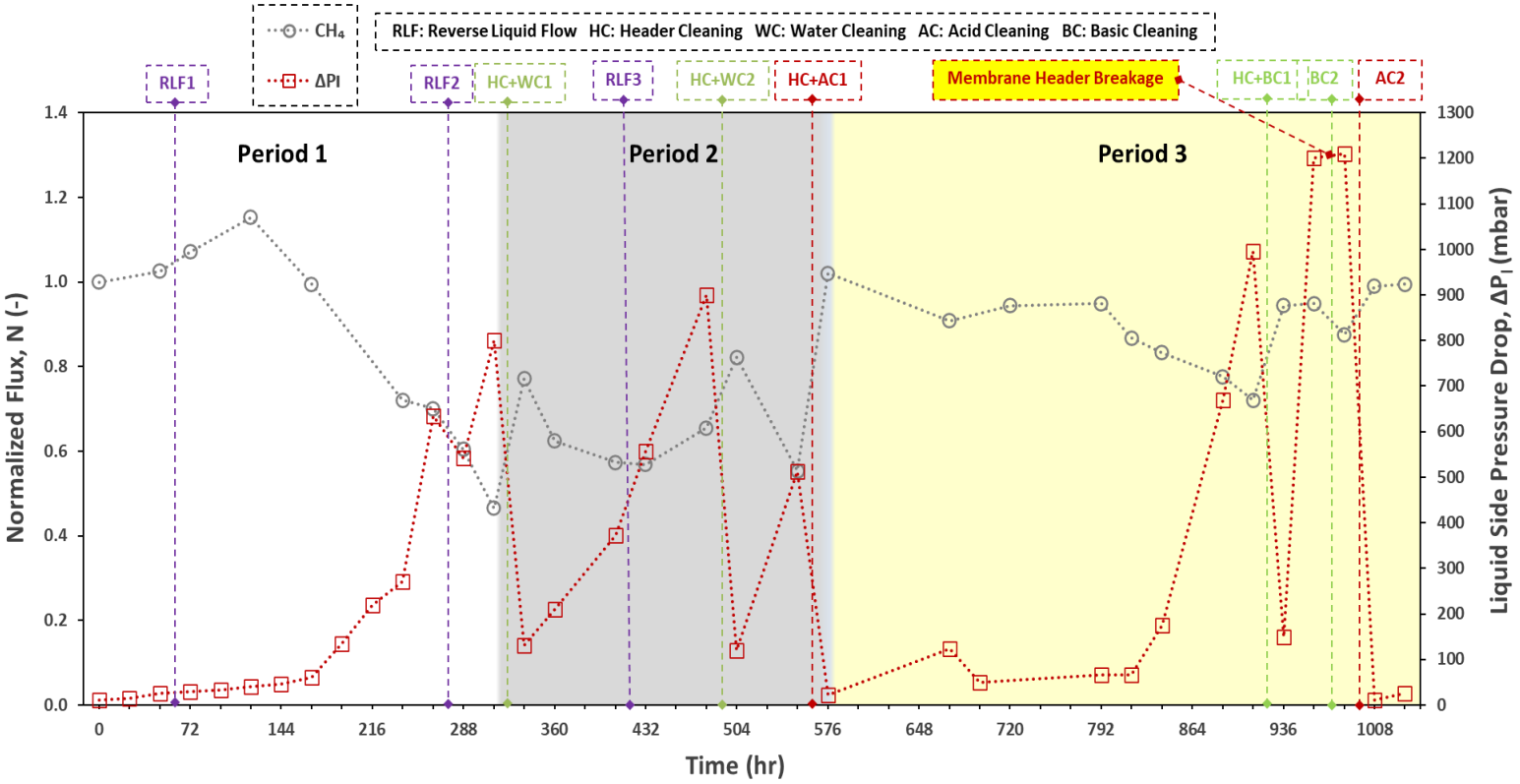

Figure 2 Loses and recoveries of the membrane contactor methane flux and liquid side pressure drop during long-term G-AnMBR effluent degassing; V_l=5.93 10^{-03} m s^{-1}, V_g=1.86 10^{-03} m s^{-1}, T= 25 °C, $P_{g,\,in}$= 1028 mbar, $P_{l,\,in}$=1113-2323 mbar.

From the above-mentioned details, it can be concluded that both reversible and irreversible fouling and/or clogging were developed during the membrane degassing of the G-AnMBR effluent. Water cleaning and basic cleaning were ineffective in long-term operation while acid cleaning was very effective in recovering the membrane performance. The effective AC and ineffective BC could be

explained by two reasons: either AC was also effective in removing major organic fouling or there was dominant inorganic fouling and less organic fouling in this case. Brant [43], while studying cleaning protocols for the organic fouled microfiltration membranes, found improvement in the results by adding a weak acid such as hydrogen peroxide to the commercial cleaning solution having caustic soda. These results also verified the effectiveness of the AC for the organic foulants.

3.1.2 Membrane degassing efficiency and 3h-recovery

Membrane degassing efficiency during the long-term G-AnMBR effluent degassing operation was calculated using Equation 2 and has been reported in Figure 3.

Here again (as of Figure 2), it can be observed that RLF had nearly no influence on the degassing efficiency and its recovery. The initial (pristine membrane) CH_4 and CO_2 degassing efficiencies were 96 % and 65 % respectively. The drop in the efficiency with operation time was very significant in Period 1, as after 312 hrs. of the operation CH_4 and CO_2 efficiencies dropped to 55 % and 32 %, respectively, which represents nearly 43 % and 51 % decrease respectively. In a study by [28], a 50 % CH_4 degassing efficiency loss has also been reported in 200hrs.

In Period 2, a WC1 restored the efficiency of CH_4 and CO_2 up to 70 % and 38 %, respectively. WC2 was performed after 480 hrs. of the operation and restored the efficiency of CH_4 and CO_2 up to 80 % and 50 %, respectively. But the efficiency restoration was very short and there was a sharp decline in the efficiency. Both WCs could not restore the initial efficiencies and hence were not able to deal with the irreversible fouling. Similar effects of the WC have also been reported by [28]. The maximum efficiency drop in our study was recorded at 480 hrs. where the CH_4 and CO_2 efficiencies dropped to 48 % and 23 %, respectively. AC1 at 552 hrs. of the operation recovered the CH_4 efficiency, while the CO_2 efficiency was 5 % lower than the initial.

In Period 3, the BC1 increased the CH_4 and CO_2 efficiency respectively from 71 to 81 and 39 to 48, but the values were still very far from the recovery. BC2 couldn't add any improvement to the efficiency recovery. AC2 was able to recover the initial degassing efficiency. The study of [28] also reported the total recovery of the efficiency with the chemical cleaning but it was not clear which chemical cleaning (AC or BC) was more effective and recommended.

It can be attributed that ACs are able to recover the initial degassing efficiency by removing both reversible and irreversible fouling. We can also attribute that ACs are able to deal with both inorganic and organic (possibly major components and not all) fouling. Both WC and BC were not very effective in recovering the degassing efficiency.

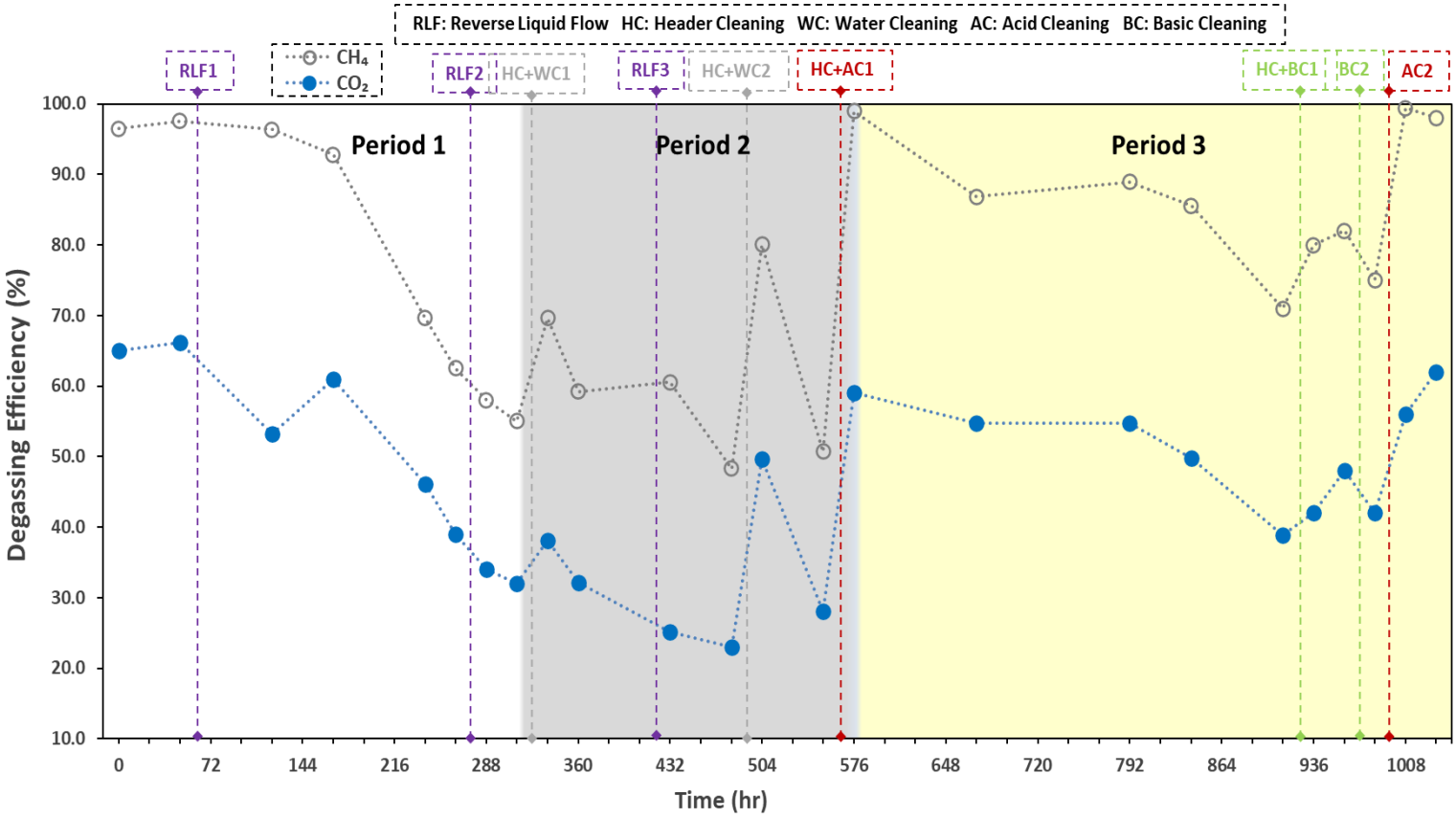

Figure 3 Loses and recoveries of the membrane contactor degassing efficiency during long-term G-AnMBR effluent degassing; V_l=5.93 10^{-03} m s^{-1}, V_g=1.86 10^{-03} m s^{-1}, T= 25 °C, $P_{g,in}$= 1028 mbar, $P_{l,in}$=1113-2323 mbar.

The biogas recovery (from the G-AnMBR effluent) percentage in the first three hours of the degassing operation during the long-term G-AnMBR effluent degassing was calculated using Equation 3 and has been reported in Figure S2 of the supplementary data. The 3h-Recovery % means the % biogas recovered from the G-AnMBR effluent during the three hours of the degassing. This was calculated from the initial biogas concentration of the effluent and concentration after 3 hrs. The initial 3h-recovery % was 84 and 75 for CH_4 and CO_2, respectively, which dropped to 32 % and 27 %, respectively, after 312 hrs (period 1). of the degassing operation. WC1 and WC2 were able to recover a part of the biogas 3h-recovery, but could not restore it to the initials. For example, WC2 brings back the 3h-recovery % from 64 to 73. Both AC1 and AC2 were very effective and recovered the 3h-recovery % to its initials. BC1 recovered only a part of the 3h-recovery % and was not as effective as AC. The reported results justify the existence of major inorganic fouling (effective AC) and also identifies the effectiveness of the AC against both inorganic and organic fouling.

3.1.3 Fouling resistance

Fouling resistances were calculated based on the comparison between the overall experimental mass transfer coefficient at time t and at the one at beginning of the experiment (Equations 6-8). Considering

that there was no change in local gas side and liquid side mass transfer coefficient nor in membrane mass transfer coefficient, the additional resistance is only due to the fouling. This fouling resistance is shown in Figure 4. Figure 4 also presents the variations in liquid side pressure drop which were also related to membrane fouling and flow clogging.

Figure 4 revealed the relation between the mass transfer resistance due to fouling (increase of the membrane fouling which limit the transmembrane flux) and the liquid side pressure drop (increase of fouling/clogging which limit the flow in the lumen side of the membrane). The trend was nearly identical as presented in the Figure 4. With the operation time, each increase in the pressure drop indicated the addition of more fouling as there was an increase in the fouling resistance too. After each cleaning step, we observed a decline in the liquid side pressure drop as well as in the fouling resistance. In the first 312 hrs. of the degassing operation (period 1), the R_f increased from 0 to 0.8, which represented a significant resistance due to fouling. We also observed that at the end of this period (312 hrs.) there was a huge increase of 800 mbar in the liquid side pressure drop, which represented the significance of membrane fouling and fiber clogging on the liquid side pressure drop.

In the Period 2, WC1 at 312 hrs. reduced the normalized R_f from 0.80 to 0.45, and ΔP_l from 800 mbar to 130 mbar. WC1 could not recover the initial R_f and the initial ΔP_l, which confirms the inefficacy of WC and also the presence of irreversible fouling. The WC2 at 480 hrs. further reduced the normalized R_f to 0.27 and ΔP_l to 120 mbar. AC was very effective, for example, AC1 at 552 hrs. recovered the initial R_f and also reduced the ΔP_l (22 mbar) to nearly its initial value (10 mbar). The effective AC indicated its efficacy against the removal of both revisable and irreversible fouling.

In Period 3, basic cleanings (at 912 hrs. and 960 hrs.) were found ineffective as it could not recover the initial R_f nor the initial ΔP_l. The ineffective BC could be because of the two reasons, dominancy of inorganic fouling over organic fouling and/or ineffectiveness of the BC against irreversible fouling.

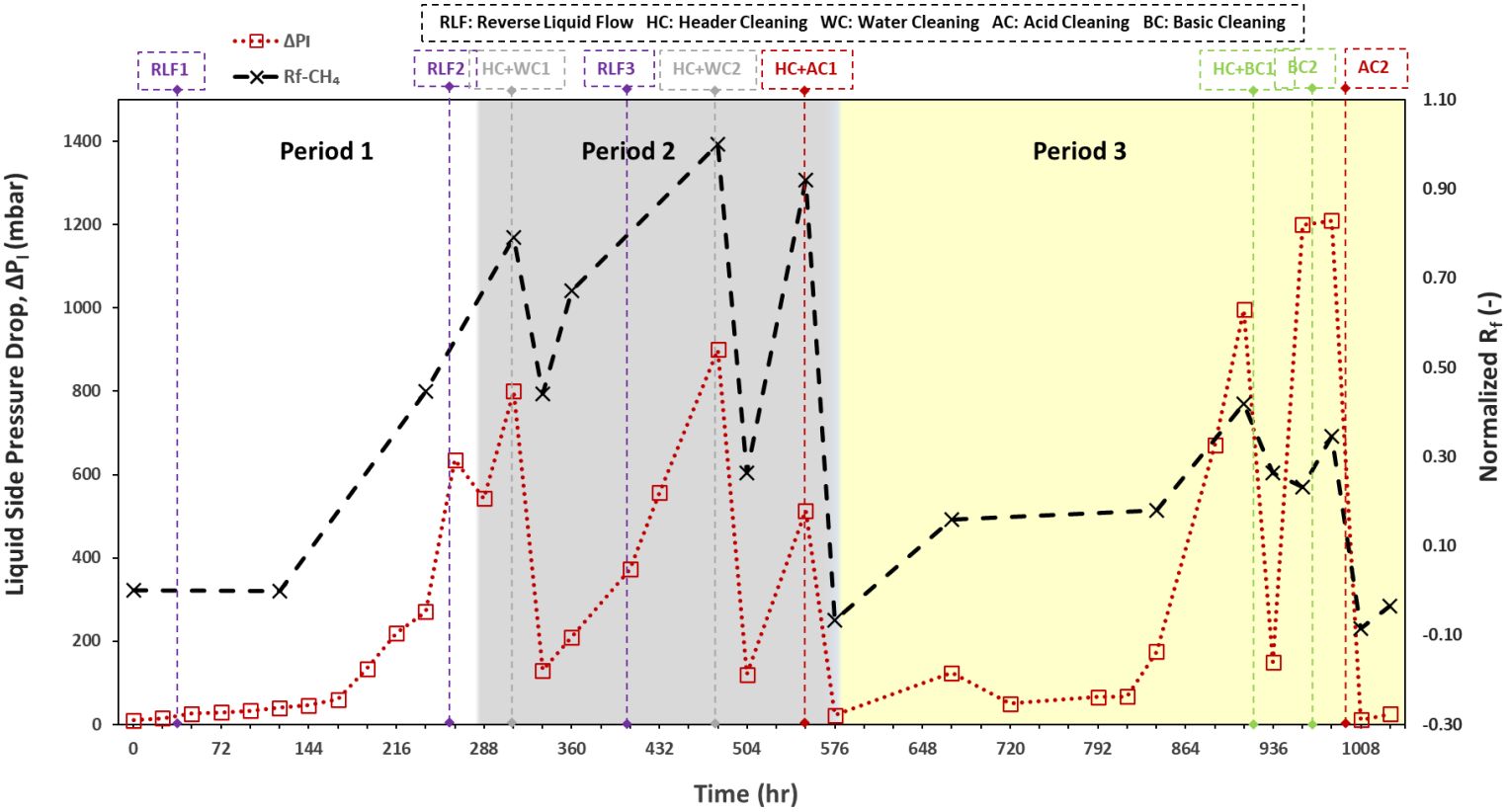

Figure 4 Variations of the liquid side pressure drop (ΔP_l) and normalized resistance due to fouling (R_f), during long-term G-AnMBR effluent degassing; V_l=5.93 10^{-03} m s^{-1}, V_g=1.86 10^{-03} m s^{-1}, T= 25 °C, $P_{g,in}$= 1028 mbar, $P_{l,in}$=1113-2323 mbar.

3.2 Fouling and foulants characterization

The performance loss (due to fouling) and recovery (due to membrane cleaning) of the membrane degassing setup have been well discussed in the Section 3.1. The results of this section identified the presence of a huge amount of fouling. To completely understand the fouling behavior and also confirm hypothesis on this fouling and cleaning mechanisms, it was needed to characterize the fouling and foulants to know their nature, location, and intensity. Here in this section various characterization techniques were implemented and are discussed.

3.2.1 Fouled membrane and fouled membrane header analysis (SEM and EDX analysis)

The preliminary study of the fouling on membrane was made using porous PP fibers (similar to the ones in the membrane contactor) immersed in discharched G-AnMBR effluent for 1 or 5 months. At initial time, at 1-month and at 5-month, SEM analysis was performed to analyze the fouled surface and morphology. Figure 5 (a, b) shows the pristine membrane surface and the membrane pores. The SEM of the membrane fiber surface after one month immersion in the G-AnMBR effluent shows that fouling mostly occurred in the form of precipitates (Figure c, d, e and f). The visual form of the 1-month fouling shows the existence of dominant inorganic fouling that might have occurred due to the precipitation

of the inorganic substances such as inorganic carbonates present in the G-AnMBR effluent. The membrane pore blockage due to the presence of foulants can be easily seen in Figure 5 (d, e, f). The SEM cannot exactly identify the nature of the foulants, therefore the existence of organic fouling cannot be ruled out at this stage. The nature of the both inorganic and organic fouling will be studied in the upcoming sections using other characterization techniques.

The after 5 months analysis (membrane immersed for 5 months in the AnMBR permeate) of the membrane fiber surface shows that the major part of the surface was covered by a thick fouling layer (Figure 5 (g)). After magnifying the 5-month fouling layer, it was found that the layer was thick, porous, and can be regarded as a cake layer (Figure 5 (h)). This porous cake layer developed on the membrane surface is mostly reversible and is expected to be removed by physical means [44].

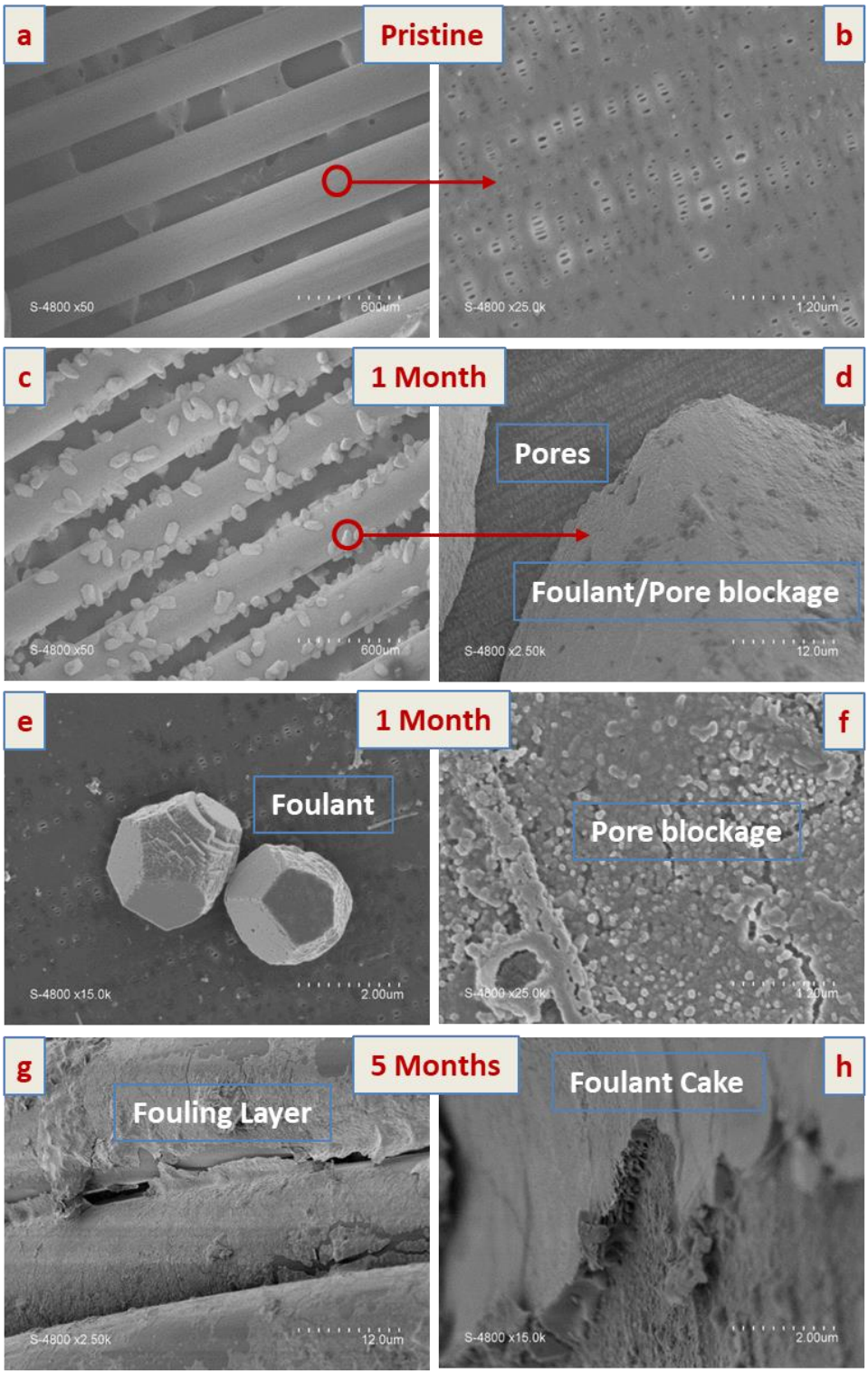

Figure 5 SEM of the porous PP membrane surface; (a, b) pristine membrane, (c, d, e, f) membrane immersed for 1 month in the G-AnMBR effluent, (g, h) membrane immersed for 5 months in the G-AnMBR effluent.

EDX analysis of the pristine PP membrane fiber, fouled PP membrane fiber, and membrane H-Foulants (foulants recover from the cleaning of the header of membrane module) were performed to analyze

and quantify the elements present in the foulants or the elements that are taking part in the fouling process. Pristine PP fiber EDX showed a composition of nearly 95 % atomic C and 5 % atomic O (Table 4) due to the polypropylene material of the fiber. Pilarska and co-workers [45] have also reported nearly the same composition in their studies. It is important to mention here that hydrogen (H) is a non-detectable element through EDX [46]. EDX of the fouled fiber and H-Foulants showed several elements present in the foulants. C, O, N, Ca, Na, and Mg were the major elements that were detected in the foulants. For the fouled fiber analysis, the C and O contents of the fouled fiber are not be totally from the foulants due to the PP fiber composition but the ones present in the H-Foulants are totally from the foulants. The huge amount of C content (up to 27 % Atomic) in the H-Foulants clearly represented the presence of organic fouling and/or carbonate precipitation. The presence of a high amount of O and the usual amount of N could be assumed as a representation of both inorganic and organic fouling. This could not be clearly identified here whether O and N present in the foulants belonged to inorganic fouling, organic fouling, or both, due to the presence of ions (like NH_4^+, NO_3^-, SO_4^{2-}, PO_4^{3-}) from various salts in the effluent. The presence of organic fouling demands a high number of N element, which was not the case here. This lower amount of N can be explained by the fact that this element was not easily detectable by EDX [46]. The huge amount of Ca in the foulants identified Ca as a major element causing inorganic fouling. Ca could also be present in the form of di-cations Ca complexes with organic foulants forming intermolecular bridges between organic foulants molecules [47]. The other major elements of the inorganic fouling were Na and Mg, while K, P, S, Cl, Si, and Al were present in small amounts. The EDX analysis identified the elements in the fouling and also gave an idea of the presence of both inorganic and organic fouling. The nature of the fouling will be further studied in detail by ions chromatography in the next section.

Table 4 EDX analysis of the pristine PP membrane fiber, fouled PP membrane fiber, and membrane header foulants

Element	Pristine fiber		Fouled fiber		Header Foulants	
	% Mass	% Atomic	% Mass	% Atomic	% Mass	% Atomic
C	91.57-92.78	93.54-94.48	10.70-18.17	24.07-36.92	13.99-16.64	23.43-26.62
O	7.22-8.43	5.52-6.46	16.09-32.17	27.72-54.33	36.77-48.41	36.23-57.75
N	-	-	-	-	5.30	5.96
Ca	-	-	9.23-10.48	6.38-6.22	17.95-41.25	7.06-20.70
Na	-	-	6.36-7.62	7.48-8.09	0.51	0.35
Mg	-	-	0.33-3.47	0.33-3.86	0.24-0.47	0.19-0.37
K			0.23-2.11	0.12-1.46	0.07	0.04
P	-	-	-	-	0.06-0.38	0.03-0.19
S	-	-	0.70-0.88	0.67	0.10-0.31	0.06-0.15

Cl	-	-	1.83-3.77	1.39-2.60	-	-
Al	-	-	-	-	0.12-0.19	0.08-0.11
Si	-	-	0.16-0.52	0.14-0.50	0.11-0.93	0.08-0.52

3.2.2 Inorganic fouling (Ion chromatography and Alkalinity)

The ion chromatography technique was used to identify and quantify the ions of inorganic fouling. Carbonate ions, CO_3^{2-}, and bicarbonate ions, HCO_3^- were quantified by alkalinity as they were non-detectable by ion chromatography. Ion chromatography and alkalinity tests were performed for the initial effluent, and 72h effluent (after recirculating 250 mL effluent through the membrane for 72 hrs. at 400 mL min^{-1}), H-Foulants dissolved in deionized water, and second post-acid cleaning solution (AC2). The initial and 72h effluents are explained in Section 2.1. The samples from the second post-AC were diluted 100 times due to the saturation of many ions in the solution. Few of the ions in Table 5 were thus not detected after this high dilution.

The drop in the conductivity of 72h effluent, signifies the reduction of inorganic ions in the effluent, which most probably had precipitated in the form of fouling. It is evident from Table 5 that Ca^{2+} was the major ion causing inorganic fouling. The amount of Ca^{2+} dropped by nearly 85 % between the initial and 72h effluents analysis. The amount that disappeared from the effluent might have been precipitated (on the membrane surface) in the form of salts with various anions from the Table 5 or it might have made a complex with the organic foulants. Wang and co-workers [48] reported the complex formation between Ca^{2+} and humic acid (HA) molecules. It was described that Ca^{2+} binds with two -COOH groups from HA which also reduces the electrostatic repulsion of the HA molecules. This duo of Ca^{2+} (also other di-cations like Mg^{2+}) and organic foulants could enhance the fouling dramatically. Also, the amount of Ca^{2+} present in the H-Foulants and second post-acid cleaning solution (even after 100 times dilution) was very high compared to other ions, which was a clear indication of it as the major inorganic (cation) foulant, in our case.

A mild concentration of Carbonate, CO_3^{2-} and very high concentration of bicarbonate, HCO_3^- ions were present in the initial effluent. Both CO_3^{2-} and HCO_3^- ions concentrations were dropped by 45 % in the 72h effluent. This drop might have occurred due to the precipitation of these ions or due to the CO_2 escape from the effluent because of the equilibrium shift. It is important to mention here that the CO_2 escape was not in a large quantity as the effluent used for the recirculation analysis was not CO_2 saturated (details from Section 2.2). The nearly similar pH vales for both initial and 72h effluents, also ruled out the possibility of CO_2 escape affecting CO_3^{2-} and HCO_3^- ions concentrations. Following the CO_2, bicarbonate and pH equilibrium, at the pH value of nearly 8.4, both initial and 72h effluents had

relative amount of 4.5 % CO_3^{2-}, 95.5 % of HCO_3^- and no dissolved CO_2. These values were also in line with the one reported by Huang and coworkers [49].

The highest quantity of the CO_3^{2-} among other ions present in the H-Foulants gave a clear indication of CO_3^{2-} precipitates in the fouling. The carbonates could be majorly in the form of calcium carbonate (present in the abundant amount), but also mildly of other cations (magnesium, sodium, potassium). The presence of HCO_3^- was not detected in the H-Foulants. The H-Foulants analysis showed the presence of a high amount of other ions like SO_4^{2-} and PO_4^{3-} anions. Small quantities of other anions like Cl^- and NO_3^- were also present in H-Foulants. A high amount of Na^+ was detected in the second post-acid cleaning solution. The results indicated the presence of a significant amount of inorganic fouling. The organic foulants characterization is followed in the coming sections.

Table 5 Ion chromatography and alkalinity of the initial effluent, 72h effluent, header foulants solution, and acid cleaning solution

Effluent type	pH	Conductivity µS cm^{-1}	Sodium (Na^+) mg L^{-1}	Ammonium (NH_4^+) mg L^{-1}	Potassium (K^+) mg L^{-1}	Magnesium (Mg^{2+}) mg L^{-1}	Calcium (Ca^{2+}) mg L^{-1}	Carbonate (CO_3^{2-}) mg L^{-1}	Bicarbonate (HCO_3^-) mg L^{-1}	Chloride (Cl^-) mg L^{-1}	Nitrate (NO_3^-) mg L^{-1}	Sulfate (SO_4^{2-}) mg L^{-1}	Phosphate (PO_4^{3-}) mg L^{-1}
Tap water	7.1	-	19.09	-	1.13	8.54	96.92	-	441.10	38.10	-	24.31	-
Initial effluent	8.40	1105	126.06	10.80	21.12	10.32	118.53	27.97	580.10	66.17	0.90	28.57	n.a.
72h effluent	8.49	800	134.85	5.53	22.88	9.36	18.76	15.48	324.00	71.59	1.16	33.11	2.84
Header Foulants	6.34	10.81	0.82	0.07	0.40	0.29	9.09	9.52	n.a.	0.93	0.88	1.48	1.40
Second post-Acid Cleaning (AC2) solution	2.22	4970	5.28	-	0.28	0.11	16.87	-	-	-	-	-	-

3.2.3 Organic Fouling (COD, DOC, TC and 3DEEM Analysis)

COD, DOC, and TOC of the initial and 72h effluents, H-Foulants solution, and acid cleaning solution were measured using method described in Section 2.6 and are presented here in Table 6. The extraction of organic matter from H-Foulants is also described in Section 2.6.

An increase was observed for COD and DOC, while processing the G-AnMBR effluent in the membrane. The 72h effluent COD and DOC values were higher than in the initial effluent. This signaled the existence of biological/bacterial activity in the membrane. Although the small pore size (0.04 µm) of the submerged membrane of the G-AnMBR reactor was not allowing the bacterial flow in the discharged effluent. However, there is a huge possibility of the ambient bacterial contact with the effluent inside the transfer line or in the membrane module. Unlike the DOC, TOC value dropped significantly from 27.9 mg L^{-1} to 7.2 mg L^{-1}. The high initial effluent value identified the presence of a huge quantity of TOC in the effluent while the significant drop in TOC identified that it majorly took part in the fouling formation inside the membrane.

H-Foulants showed a value of 44.3 mg L^{-1} for COD, and 10.10 mg L^{-1} for DOC, which signified the presence of substantial amount of organic fouling. The COD of the membrane acid cleaning solution was not measurable by the standard method presented in Section 2.6. The DOC and TOC values for AC were abnormally very high and unreasonable.

Table 06 Chemical oxygen demand (COD), dissolved organic carbon (DOC), and total organic carbon (TOC) of initial- and 72h effluents, membrane header foulants (H-Foulants), and acid cleaning solution (AC)

Parameter	Initial effluent	72h effluent	H-Foulants	AC
COD (mg L^{-1})	27 ± 2	34 ± 2	44.3 ± 3	Not measurable
DOC (mg L^{-1})	3.25 ± 1	8.49 ± 1.5	10.10 ± 2	31377
TOC (mg L^{-1})	27.9 ± 2	7.2 ± 1	-	31509

3DEEM fluorescence spectra and normalized fluorescence volume of different 3DEEM regions for the discharched G-AnMBR permeate (20X diluted), membrane contactor H-Foulants solution (ten times dilution of the organic matter extracted solution), and post-acid cleaning solution (five times dilution) were obtained as of the method described in Section 2.6 are presented in Figure 6 below. 3DEEM is a convenient method, providing vast fingerprinting information about the composition and nature of dissolved organic matter (DOM) [50]. Because of the different chemical compositions of the DOM, the fluorescence spectra are distributed in different regions of excitation/emission (Ex/Em). Florescence

regional integration (FRI) helps integrate the fluorescence intensity of each region and provides information about the regional contribution to the total fluorescence. According to the FRI, the fluorescence spectra of this study were divided into five regions, as presented in Table 7.

It can be observed from Figure 6 (a) that nearly 63 % (based on the normalized volume) of the DOM present in the discharched G-AnMBR effluent belonged to region III and V. Region III and V respectively represents Fulvic-like substances and Humic acid-like substances. The aromatic proteins (region I and II) were nearly 35 % of the total DOM. The SMP (region IV) ratio was comparatively very low.

Figure 6 (b) presents the fluorescence spectra and regional intensity of the DOM present in the membrane H-Foulants. The regional distribution and intensity of the DOM in the H-Foulants clearly identified which region contributed more to the fouling. Nearly 80 % of the DOM found in the H-Foulants were from the region I and II which belongs to aromatic proteins. It can also be observed from Table 7, that extracellular polymeric substance (EPS) existed at Ex < 230 nm and Em = 280–330 nm, have a strong fouling propensity. Liu and co-workers [51] has also reported that proteins and protein-like substances are the major external foulants forming a foulant layer. Fulvic-like substances and Humic acid-like substances contributed nearly 17 % to the fouling. Ly & Hur [52] also reported a small overall contribution of humic-like substances to the total fouling, and they were the dominant source of internal fouling. These substances are reported to be hydrophobic and thus induce more fouling on the hydrophobic membrane more [42]. Singh [53] found that the presence of Ca^{2+} (which was present in a high amount in our case) intensified the fouling due to the formation of a bridge between the membrane and the membrane surface (negatively charged), and/or between the membrane surface and carboxyl groups of the humic acid. The SMP's contribution to the fouling was only 4 % which was comparatively low. The SMPs were majorly causing the external fouling as of the Ex/Em range in Table 7.

As mentioned in Section 3.1.1, the acid cleaning was very effective to recover the membrane performance and remove both reversible and irreversible fouling. Therefore, the post-AC solution was analyzed by 3DEEM to observe its effectiveness against the DOM. Figure 6(c) shows that 35 % of the DOM present in the post-acid cleaning solution were from region I+II, Aromatic proteins. It is justifiable as a major part of the DOM in the foulants (Figure 6 (b)) were proteins. It also provided evidence that acid cleaning was able to dissolve aromatic proteins (but we could not verify the extent of dissolution). The humic-like substances (fulvic and humic acid) were 50 % (of which 33 % were fulvic acids) of the total DOM in the post acid cleaning solution. This result provided evidence of the AC to be very effective against region III DOM (fulvic acids). This was also due to the fact that fulvic acids are soluble in water at nearly all pH conditions [54]. The SMPs in the AC cleaning solution were 15 %, which were

comparatively low, but it is important to note that the total contribution of the SMPs in the H-Foulants were only 4 % (Figure 6 (b)). It can be concluded that like inorganic fouling (Section 3.2.2), AC was also effective in dealing with organic fouling.

Table 7 3DEEM Regions, location, biodegradable and fouling behavior [41,50,51,55].

Composition		**Biodegradation behavior**		**Fouling behavior**	
Excitation (nm) Emission (nm)	**Nature Properties**	**Excitation (nm) Emission (nm)**	**Nature Properties**	**Excitation (nm) Emission (nm)**	**Nature Properties**
Ex < 250 nm Em < 380 nm	**Region I+II** Aromatic proteins such as tyrosine-like and tryptophan-like substances	Ex < 230 nm Em = 280–330 nm	EPS-like substances	Ex < 280 nm Em 280-330 nm	Strong fouling propensity
Ex < 250 nm Em > 380 nm	**Region III** Fulvic-like substances	Ex > 230 nm Em = 280–330 nm	SMP-like substances	Ex 200-350 nm Em 400-500 nm	Moderate fouling
Ex > 250 nm Em < 380 nm	**Region IV** Soluble microbial byproduct-like substances (SMPs)	-	-	Ex 275 nm Em 440-445 nm	Internal fouling (inside the membrane pores)
Ex > 250 nm Em > 380 nm	**Region V** Humic acid-like substances	-	-	Ex/Em 230/350 nm Ex/Em 280/345 nm	External fouling (layer formation on the surface of the membrane)

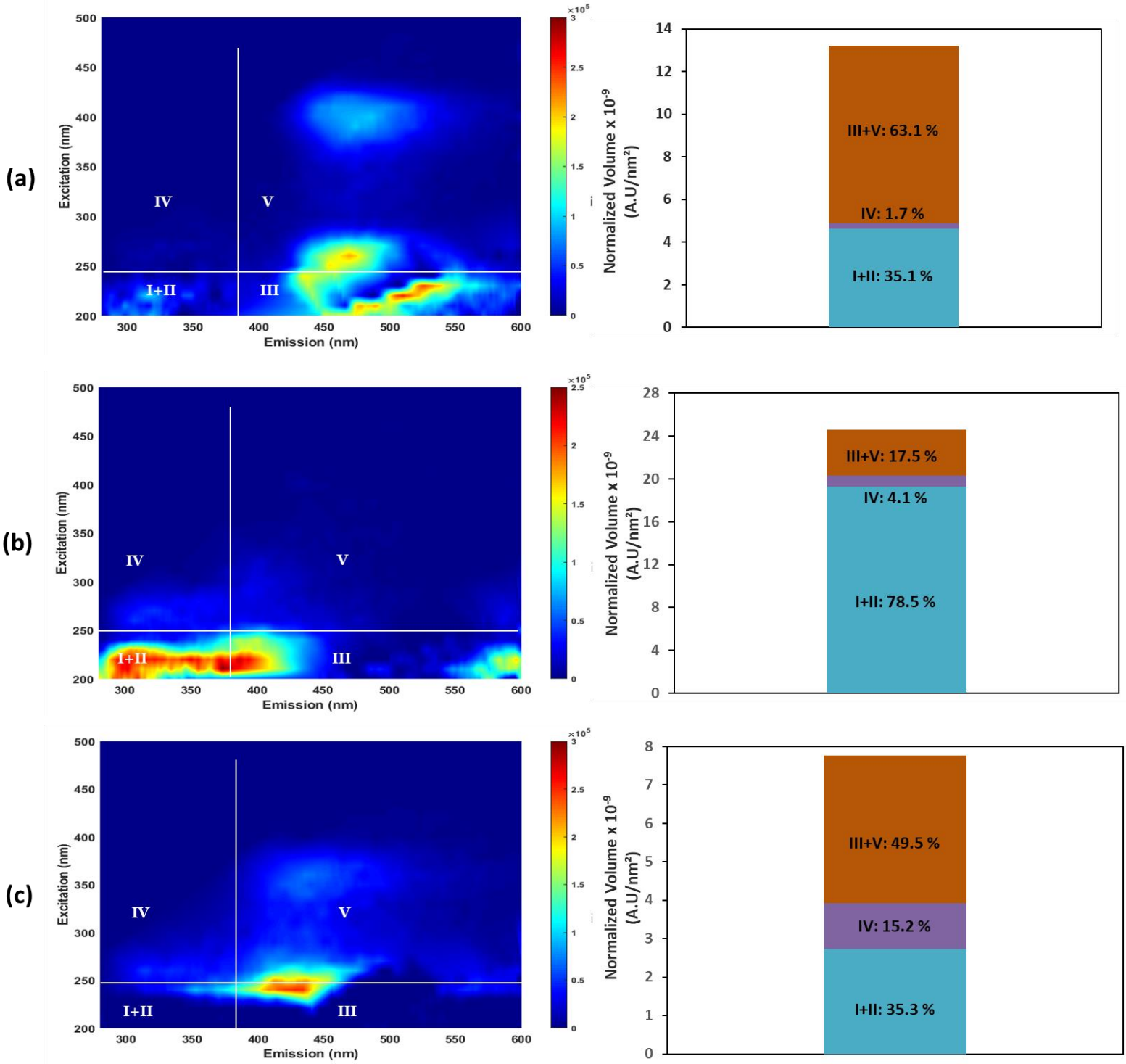

Figure 6 3DEEM fluorescence spectra (left) and normalized fluorescence volume (right) of different 3DEEM regions for the (a) G-AnMBR permeate (20X diluted); (b) membrane contactor H-Foulants (10X diluted organic matter extracted solution); (c) post-AC solution (5X diluted).

3.2.4 Combined organic and inorganic fouling (FTIR analysis)

FTIR analysis of the H-Foulants was performed to further characterize the organic foulants and also to know the inorganic precipitates as the carbonate ions (which were expected to be a major part of the

inorganic fouling) were not detectable by the ion chromatography. The method is presented in Section 2.6 and the FTIR spectra can be seen below in Figure 7.

The peak at 3290 Cm^{-1}, corresponded to the O-H/NH stretch of the primary amide, amide a, which represented proteins. These amides were likely derived from either polysaccharides or proteins [56,57]. The peak at 2960 Cm^{-1} represented the asymmetric CH_3 (Methyl C-H asym) stretch while the peak at 2510 Cm^{-1} represented the symmetric stretching modes of NH_3^+ groups [58]. The peak at 1790 Cm^{-1} represented the C=O of the acyl halides [59]. Acyl halides react with water, and ammonia, forming, carboxylic acids, and amides, respectively. The peak at 1640 Cm^{-1} represented the C=O of the amide I group, the unique spectrum of protein secondary structures [58]. The peak at 1390 Cm^{-1} represented the asymmetric stretch of CO_3^{-2} of the calcite (calcium carbonate phase) [60] or symmetric and asymmetric bending of CH_2, CH_3 / C-O of proteins/carboxylic groups [61]. The presence of nucleic acid (NA) was confirmed by the peak at 1260 Cm^{-1}. Here again, the presence of NA evidenced the existence of biofouling. The presence of polysaccharides or polysaccharides-like substances was confirmed by the C=O stretch at 1070 Cm^{-1} [58]. The large peak at 870 Cm^{-1} and the peak at 711 Cm^{-1}, represented the bending of CO_3^{-2} and the presence of calcites. The peak at 796 Cm^{-1} was probably one of the inorganic carbonates (IOC) [62].

The above-mentioned results suggested the significant existence of both inorganic and organic fouling and the probable existence of biofouling. The inorganic fouling existed majorly in the form of IOCs most likely calcites. The organic fouling majorly existed in the form of proteins and polysaccharides.

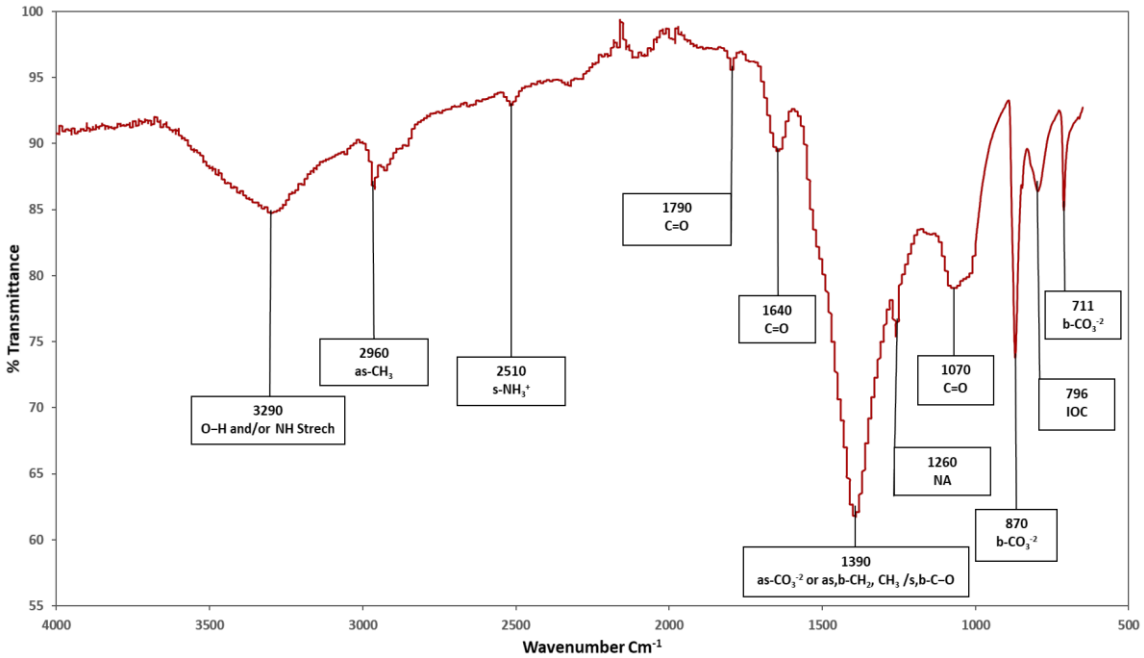

Figure 7 FTIR spectra of the membrane header foulants

4 Conclusion

A study was conducted to analyze the long-term porous PP membrane contactor degassing operation of the ultrafiltration effluent discharged from the in-house G-AnMBR unit. To perform the long-term analysis, the degassing operation was conducted for 1032 hrs., in total. During this operational time, water and chemical cleaning strategies were implemented to deal with the reversible and irreversible fouling and clogging. The variations (due to fouling) in the performance parameters were evaluated, and the characterization techniques were implemented to identify and quantify the fouling.

The normalized CH_4 flux and CH_4 degassing efficiency after 312 hrs. of without cleaning operation recorded a 54 % and 44 % drop, respectively, of the initial value for the pristine membrane. The normalized fouling resistance during this operation time increased from 0 to 0.8 while the pressure drop increased from 10 to 800 mbar. At 984 hrs. the liquid side pressure drop increased to as high as 1012 mbar, where the membrane header broke and developed a leak. AC was very effective in removing both reversible and irreversible fouling and restoring the initial membrane performance while WC and BC were ineffective in long-term operation and could not restore the initial performance. The inorganic fouling was detected to be majorly caused due to the ions including Ca^{2+}, CO_3^{2-}, HCO_3^-, which clearly represented the dominancy of carbonates. Substantial amount of organic content was detected fouling. The H-Foulants were mainly comprised of aromatic proteins and EPS (79 %), fulvic-like substances and humic acid-like substances (17 %), and SMP's (4%). The existence of the biological/bacterial activity was confirmed by the increase in the COD and DOC in the 72h effluent and also by the detection of nucleic acids in the FTIR analysis.

The study suggests regular cleaning of the membrane to avoid performance loss and membrane damage due to fouling and clogging. AC cleaning was found to be very effective in resorting membrane performance, however a more sustainable and green cleaning method is needed to be developed.

Acknowledgements

The authors acknowledge the financial support for this work, obtained from the French National Research Agency (ANR) as part of the "JCJC" Program BàMAn (ANR-18-CE04-0001-01).

References

[1] P.L. McCarty, J. Bae, J. Kim, Domestic wastewater treatment as a net energy producer-can this be achieved?, Environmental Science and Technology. (2011). https://doi.org/10.1021/es2014264.

[2] M. Maaz, M. Yasin, M. Aslam, G. Kumar, A.E. Atabani, M. Idrees, F. Anjum, F. Jamil, R. Ahmad, A.L. Khan, G. Lesage, M. Heran, J. Kim, Anaerobic membrane bioreactors for wastewater

treatment: Novel configurations, fouling control and energy considerations, Bioresource Technology. (2019). https://doi.org/10.1016/j.biortech.2019.03.061.
[3] W. Wang, Q. Yang, S. Zheng, D. Wu, Anaerobic membrane bioreactor (AnMBR) for bamboo industry wastewater treatment, Bioresource Technology. (2013). https://doi.org/10.1016/j.biortech.2013.09.068.
[4] T. Xia, X. Gao, C. Wang, X. Xu, L. Zhu, An enhanced anaerobic membrane bioreactor treating bamboo industry wastewater by bamboo charcoal addition: Performance and microbial community analysis, Bioresource Technology. (2016). https://doi.org/10.1016/j.biortech.2016.08.057.
[5] M. Aslam, P.L. McCarty, C. Shin, J. Bae, J. Kim, Low energy single-staged anaerobic fluidized bed ceramic membrane bioreactor (AFCMBR) for wastewater treatment, Bioresource Technology. (2017). https://doi.org/10.1016/j.biortech.2017.03.017.
[6] L. Sanchez, M. Carrier, J. Cartier, C. Charmette, J.-P. Steyer, M. Heran, G. Lesage, Enhanced Organic Degradation and Biogas Production of Domestic Wastewater at Psychrophilic Temperature Through Submerged Granular Anaerobic Membrane Bioreactor for Energy-Positive Treatment, SSRN Electronic Journal. (2022). https://doi.org/10.2139/ssrn.4043779.
[7] M. Aslam, R. Ahmad, M. Yasin, A.L. Khan, M.K. Shahid, S. Hossain, Z. Khan, F. Jamil, S. Rafiq, M.R. Bilad, J. Kim, G. Kumar, Anaerobic membrane bioreactors for biohydrogen production: Recent developments, challenges and perspectives, Bioresource Technology. (2018). https://doi.org/10.1016/j.biortech.2018.08.050.
[8] B.Q. Liao, J.T. Kraemer, D.M. Bagley, Anaerobic membrane bioreactors: Applications and research directions, Critical Reviews in Environmental Science and Technology. (2006). https://doi.org/10.1080/10643380600678146.
[9] B.C. Crone, J.L. Garland, G.A. Sorial, L.M. Vane, Significance of dissolved methane in effluents of anaerobically treated low strength wastewater and potential for recovery as an energy product: A review, Water Research. (2016). https://doi.org/10.1016/j.watres.2016.08.019.
[10] G.S.M.D.P. Sethunga, H.E. Karahan, R. Wang, T.H. Bae, PDMS-coated porous PVDF hollow fiber membranes for efficient recovery of dissolved biomethane from anaerobic effluents, Journal of Membrane Science. (2019). https://doi.org/10.1016/j.memsci.2019.05.016.
[11] S. Heile, C.A.L. Chernicharo, E.M.F. Brandt, E.J. McAdam, Dissolved gas separation for engineered anaerobic wastewater systems, Separation and Purification Technology. (2017). https://doi.org/10.1016/j.seppur.2017.08.021.
[12] J. Cookney, A. Mcleod, V. Mathioudakis, P. Ncube, A. Soares, B. Jefferson, E.J. McAdam, Dissolved methane recovery from anaerobic effluents using hollow fibre membrane contactors, Journal of Membrane Science. (2016). https://doi.org/10.1016/j.memsci.2015.12.037.
[13] P. Sanchis-Perucho, Á. Robles, F. Durán, J. Ferrer, A. Seco, PDMS membranes for feasible recovery of dissolved methane from AnMBR effluents, Journal of Membrane Science. (2020). https://doi.org/10.1016/j.memsci.2020.118070.
[14] J. Cookney, E. Cartmell, B. Jefferson, E.J. McAdam, Recovery of methane from anaerobic process effluent using poly-di-methyl-siloxane membrane contactors, Water Science and Technology. (2012). https://doi.org/10.2166/wst.2012.897.
[15] B.C. Crone, J.L. Garland, G.A. Sorial, L.M. Vane, Significance of dissolved methane in effluents of anaerobically treated low strength wastewater and potential for recovery as an energy product: A review, Water Research. (2016). https://doi.org/10.1016/j.watres.2016.08.019.
[16] T.E. Rufford, S. Smart, G.C.Y. Watson, B.F. Graham, J. Boxall, J.C. Diniz da Costa, E.F. May, The removal of CO 2 and N 2 from natural gas: A review of conventional and emerging process technologies, Journal of Petroleum Science and Engineering. (2012). https://doi.org/10.1016/j.petrol.2012.06.016.
[17] A. Mansourizadeh, A.F. Ismail, Hollow fiber gas–liquid membrane contactors for acid gas capture: A review, Journal of Hazardous Materials. 171 (2009) 38–53. https://doi.org/10.1016/j.jhazmat.2009.06.026.

[18] M. Younas, T. Tahir, C. Wu, S. Farrukh, Q. Sohaib, A. Muhammad, M. Rezakazemi, J. Li, Post-combustion CO2capture with sweep gas in thin film composite (TFC) hollow fiber membrane (HFM) contactor, Journal of CO2 Utilization. (2020). https://doi.org/10.1016/j.jcou.2020.101266.
[19] Q. Sohaib, J.M. Vadillo, L. Gómez-Coma, J. Albo, S. Druon-Bocquet, A. Irabien, J. Sanchez-Marcano, CO2 capture with room temperature ionic liquids; coupled absorption/desorption and single module absorption in membrane contactor, Chemical Engineering Science. (2020). https://doi.org/10.1016/j.ces.2020.115719.
[20] M. Henares, M. Izquierdo, P. Marzal, V. Martínez-Soria, Demethanization of aqueous anaerobic effluents using a polydimethylsiloxane membrane module: Mass transfer, fouling and energy analysis, Separation and Purification Technology. (2017). https://doi.org/10.1016/j.seppur.2017.05.035.
[21] Z. Dai, L. Deng, Membrane absorption using ionic liquid for pre-combustion CO 2 capture at elevated pressure and temperature, International Journal of Greenhouse Gas Control. 54 (2016) 59–69. https://doi.org/10.1016/j.ijggc.2016.09.001.
[22] S. Mosadegh-Sedghi, D. Rodrigue, J. Brisson, M.C. Iliuta, Wetting phenomenon in membrane contactors – Causes and prevention, Journal of Membrane Science. 452 (2014) 332–353. https://doi.org/10.1016/j.memsci.2013.09.055.
[23] Q. Sohaib, J.M. Vadillo, L. Gómez-Coma, J. Albo, S. Druon-Bocquet, A. Irabien, J. Sanchez-Marcano, Post-combustion CO2 capture by coupling [emim] cation based ionic liquids with a membrane contactor; Pseudo-steady-state approach, International Journal of Greenhouse Gas Control. (2020). https://doi.org/10.1016/j.ijggc.2020.103076.
[24] M. Zhang, B. qiang Liao, X. Zhou, Y. He, H. Hong, H. Lin, J. Chen, Effects of hydrophilicity/hydrophobicity of membrane on membrane fouling in a submerged membrane bioreactor, Bioresource Technology. (2015). https://doi.org/10.1016/j.biortech.2014.10.058.
[25] Y. Chun, D. Mulcahy, L. Zou, I.S. Kim, P. Le-Clech, Influence of hydrophobic and electrostatic membrane surface properties on biofouling in a submerged membrane bioreactor under different filtration modes, Desalination and Water Treatment. (2016). https://doi.org/10.1080/19443994.2016.1189707.
[26] Q. Sohaib, C. Kalakech, C. Charmette, J. Cartier, G. Lesage, J.P. Mericq, Hollow-Fiber Membrane Contactor for Biogas Recovery from Real Anaerobic Membrane Bioreactor Permeate, Membranes. 12 (2022). https://doi.org/10.3390/membranes12020112.
[27] I. Ruigómez, L. Vera, E. González, G. González, J. Rodríguez-Sevilla, A novel rotating HF membrane to control fouling on anaerobic membrane bioreactors treating wastewater, Journal of Membrane Science. (2016). https://doi.org/10.1016/j.memsci.2015.12.011.
[28] M. Henares, P. Ferrero, P. San-Valero, V. Martínez-Soria, M. Izquierdo, Performance of a polypropylene membrane contactor for the recovery of dissolved methane from anaerobic effluents: Mass transfer evaluation, long-term operation and cleaning strategies, Journal of Membrane Science. (2018). https://doi.org/10.1016/j.memsci.2018.06.045.
[29] P. Ferrero, P. San-Valero, C. Gabaldón, V. Martínez-Soria, J.M. Penya-roja, Anaerobic degradation of glycol ether-ethanol mixtures using EGSB and hybrid reactors: Performance comparison and ether cleavage pathway, Journal of Environmental Management. (2018). https://doi.org/10.1016/j.jenvman.2018.02.070.
[30] D.C. Stuckey, Recent developments in anaerobic membrane reactors, Bioresource Technology. (2012). https://doi.org/10.1016/j.biortech.2012.05.138.
[31] Z. Huang, S.L. Ong, H.Y. Ng, Submerged anaerobic membrane bioreactor for low-strength wastewater treatment: Effect of HRT and SRT on treatment performance and membrane fouling, Water Research. (2011). https://doi.org/10.1016/j.watres.2010.08.035.
[32] M. Aslam, R. Ahmad, J. Kim, Recent developments in biofouling control in membrane bioreactors for domestic wastewater treatment, Separation and Purification Technology. (2018). https://doi.org/10.1016/j.seppur.2018.06.004.
[33] W.M.K.R.T.W. Bandara, H. Satoh, M. Sasakawa, Y. Nakahara, M. Takahashi, S. Okabe, Removal of residual dissolved methane gas in an upflow anaerobic sludge blanket reactor treating low-

strength wastewater at low temperature with degassing membrane, Water Research. (2011). https://doi.org/10.1016/j.watres.2011.04.030.
[34] W. Rongwong, K. Goh, G.S.M.D.P. Sethunga, T.H. Bae, Fouling formation in membrane contactors for methane recovery from anaerobic effluents, Journal of Membrane Science. (2019). https://doi.org/10.1016/j.memsci.2018.12.038.
[35] Q. Sohaib, C. Kalakech, C. Charmette, J. Cartier, G. Lesage, J.-P. Mericq, Hollow-Fiber Membrane Contactor for Biogas Recovery from Real Anaerobic Membrane Bioreactor Permeate, Membranes. 12 (2022) 112. https://doi.org/10.3390/membranes12020112.
[36] M. Layer, A. Adler, E. Reynaert, A. Hernandez, M. Pagni, E. Morgenroth, C. Holliger, N. Derlon, Organic substrate diffusibility governs microbial community composition, nutrient removal performance and kinetics of granulation of aerobic granular sludge, Water Research X. (2019). https://doi.org/10.1016/j.wroa.2019.100033.
[37] S.B. Iversen, V.K. Bhatia, K. Dam-Johansen, G. Jonsson, Characterization of microporous membranes for use in membrane contactors, Journal of Membrane Science. 130 (1997) 205–217. https://doi.org/10.1016/S0376-7388(97)00026-4.
[38] Y. Yu, J.A. Ramsay, B.A. Ramsay, On-line estimation of dissolved methane concentration during methanotrophic fermentations, Biotechnology and Bioengineering. (2006). https://doi.org/10.1002/bit.21050.
[39] R. Sander, Compilation of Henry's law constants (version 4.0) for water as solvent, Atmospheric Chemistry and Physics. 15 (2015) 4399–4981. https://doi.org/10.5194/acp-15-4399-2015.
[40] E.M. Carstea, J. Bridgeman, A. Baker, D.M. Reynolds, Fluorescence spectroscopy for wastewater monitoring: A review, Water Research. (2016). https://doi.org/10.1016/j.watres.2016.03.021.
[41] W. Chen, P. Westerhoff, J.A. Leenheer, K. Booksh, Fluorescence Excitation-Emission Matrix Regional Integration to Quantify Spectra for Dissolved Organic Matter, Environmental Science and Technology. (2003). https://doi.org/10.1021/es034354c.
[42] C. Jacquin, G. Lesage, J. Traber, W. Pronk, M. Heran, Three-dimensional excitation and emission matrix fluorescence (3DEEM) for quick and pseudo-quantitative determination of protein- and humic-like substances in full-scale membrane bioreactor (MBR), Water Research. (2017). https://doi.org/10.1016/j.watres.2017.04.009.
[43] J.A. Brant, P. Kwan, U. Daniel, R. Valencia, Pilot-Scale Evaluation of Chemical Cleaning Protocols for Organic and Biologically Fouled Microfiltration Membranes, Journal of Environmental Engineering. (2010). https://doi.org/10.1061/(asce)ee.1943-7870.0000192.
[44] K. Calderón, B. Rodelas, N. Cabirol, J. González-López, A. Noyola, Analysis of microbial communities developed on the fouling layers of a membrane-coupled anaerobic bioreactor applied to wastewater treatment, Bioresource Technology. (2011). https://doi.org/10.1016/j.biortech.2011.01.007.
[45] A. Pilarska, K. Bula, K. Myszka, T. Rozmanowski, K. Szwarc-Rzepka, K. Pilarski, Ł. Chrzanowski, K. Czaczyk, T. Jesionowski, Functional polypropylene composites filled with ultra-fine magnesium hydroxide, Open Chemistry. (2015). https://doi.org/10.1515/chem-2015-0024.
[46] W.J. Wolfgong, Chemical analysis techniques for failure analysis, in: Handbook of Materials Failure Analysis with Case Studies from the Aerospace and Automotive Industries, 2016. https://doi.org/10.1016/b978-0-12-800950-5.00015-6.
[47] B. Mi, M. Elimelech, Chemical and physical aspects of organic fouling of forward osmosis membranes, Journal of Membrane Science. (2008). https://doi.org/10.1016/j.memsci.2008.04.036.
[48] Z. Wang, Y. Li, P. Song, X. Wang, NaCl cleaning of 0.1 Mm polyvinylidene fluoride (PVDF) membrane fouled with humic acid (HA), Chemical Engineering Research and Design. (2018). https://doi.org/10.1016/j.cherd.2018.01.009.
[49] P.M. Huang, Y. Li, M.E. Sumner, Handbook of soil sciences: resource management and environmental impacts, CRC Press, Boca Raton, Fla., 2011. http://www.crcnetbase.com/isbn/9781439803080 (accessed August 8, 2022).

[50] J. Yu, K. Xiao, W. Xue, Y. xiao Shen, J. Tan, S. Liang, Y. Wang, X. Huang, Excitation-emission matrix (EEM) fluorescence spectroscopy for characterization of organic matter in membrane bioreactors: Principles, methods and applications, Frontiers of Environmental Science and Engineering. (2020). https://doi.org/10.1007/s11783-019-1210-8.

[51] T. Liu, Z. lin Chen, W. zheng Yu, S. jie You, Characterization of organic membrane foulants in a submerged membrane bioreactor with pre-ozonation using three-dimensional excitation-emission matrix fluorescence spectroscopy, Water Research. (2011). https://doi.org/10.1016/j.watres.2010.12.023.

[52] Q.V. Ly, J. Hur, Further insight into the roles of the chemical composition of dissolved organic matter (DOM) on ultrafiltration membranes as revealed by multiple advanced DOM characterization tools, Chemosphere. 201 (2018) 168–177. https://doi.org/10.1016/j.chemosphere.2018.02.181.

[53] R. Singh, Membrane Technology and Engineering for Water Purification: Application, Systems Design and Operation: Second Edition, 2014. https://doi.org/10.1016/C2013-0-15275-0.

[54] A.A. Chaaban, Study of the structural organization of humic nanocolloids, Université Paul Sabatier - Toulouse III, 2016.

[55] K. Xiao, S. Liang, A. Xiao, T. Lei, J. Tan, X. Wang, X. Huang, Fluorescence quotient of excitation-emission matrices as a potential indicator of organic matter behavior in membrane bioreactors, Environmental Science: Water Research and Technology. (2018). https://doi.org/10.1039/c7ew00270j.

[56] K. Lim, Anaerobic membrane bioreactors for domestic wastewater treatment: Treatment performance and fouling characterization, California State Polytechnic University, 2016.

[57] H. Chen, S. Chang, Q. Guo, Y. Hong, P. Wu, Brewery wastewater treatment using an anaerobic membrane bioreactor, Biochemical Engineering Journal. (2016). https://doi.org/10.1016/j.bej.2015.10.006.

[58] D. Chen, M. Liu, L. Yin, T. Li, Z. Yang, X. Li, B. Fan, H. Wang, R. Zhang, Z. Li, H. Xu, H. Lu, D. Yang, J. Sun, L. Gao, Single-crystalline MoO3 nanoplates: Topochemical synthesis and enhanced ethanol-sensing performance, Journal of Materials Chemistry. (2011). https://doi.org/10.1039/c1jm11447f.

[59] W.H.W. Liu, Traditional Herbal Medicine Research Methods: Identification, Analysis, Bioassay, and Pharmaceutical and Clinical Studies, 2010. https://doi.org/10.1002/9780470921340.

[60] P.Y. Sow, IR - Spectroscopic Investigations of the Kinetics of Calcium Carbonate Precipitation, University of Konstanz, 2016.

[61] J.J. Mayers, K.J. Flynn, R.J. Shields, Rapid determination of bulk microalgal biochemical composition by Fourier-Transform Infrared spectroscopy, Bioresource Technology. (2013). https://doi.org/10.1016/j.biortech.2013.08.133.

[62] S. Daniilia, E. Minopoulou, K.S. Andrikopoulos, A. Tsakalof, K. Bairachtari, From Byzantine to post-Byzantine art: the painting technique of St Stephen's wall paintings at Meteora, Greece, Journal of Archaeological Science. (2008). https://doi.org/10.1016/j.jas.2008.03.017.